FCTUC FACULDADE DE CIÊNCIAS
E TECNOLOGIA
UNIVERSIDADE DE COIMBRA

DEPARTAMENTO DE
ENGENHARIA MECÂNICA

Improvement of a CNC Automation Approach in AFM (Atomic Force Microscopy) Probe-Based Machining

Submitted in Partial Fulfilment of the Requirements for the Degree of Master in Mechanical Engineering in the speciality of Production and Project

Author

Francisco Xavier de Basto Goulão Machado

Advisors

Maria Fátima da Costa Paulino

Stéphane Thiery

Jury

President	**Professor Doutor José Luís Ferreira Afonso** **Professor Auxiliar da Universidade de Coimbra**
Vowels	**Professor Doutor Fábio Jorge Pereira Simões** **Professor Adjunto do Instituto Politécnico de Leiria**
	Professora Doutora Ana Paula Bettencourt Martins Amaro **Professora Auxiliar da Universidade de Coimbra**
Advisor	**Engenheira Maria Fátima da Costa Paulino** **Assistente Convidada da Universidade de Coimbra**

Institutional Collaboration

Universidade de Coimbra

École Nationale Supérieure d'Arts et Métiers

Coimbra, September, 2015

To my parents, brother, Diogo, and nephew, Bernardo, and to my girlfriend, Beatriz.

ACKNOWLEDGEMENTS

Foremost, I would like to express my sincere gratitude to my supervisor in Lille, Dr. Stéphane Thiery for his continuous support since the beginning of this project. His motivation and generous guidance turn all the things possible for me to work on a project that, since very early, was of great interest to me. Also his huge patience to explain me the subject with which I was not so comfortable with, was of great value to me.

I am also thoroughly grateful to Dr. Emmanuel Brousseau, my supervisor in Cardiff for sharing his expertise with me, especially in an area that was very hard for me, that is to say machining and tribology. His remarks, both at a professional and personal level, were of great importance to me. Moreover, his PhD. Student, Mr. Raheem Al-Musawi was a really tireless friend and since the beginning of my project gave me really useful guidelines in how to handle the Atomic Force Microscope.

I would also like to thanks my other supervisors, Dr. Olivier Gibaru, Dr. Erick Nyiri and Professora Maria de Fátima Paulino who were always available to give me the best possible advices to develop my project.

This project would not be possible to be carried out without the partnership between Cardiff School of Engineering and Arts et Métiers ParisTech Lille. Thus, a big thanks to these two enormous Institutions.

This project is also dedicated to all my KIMP colleagues and Professors, as well as to all the workers of the Automation Laboratory on ENSAM, Lille.

I am hugely indebted to my two flatmates and long time friends, Gil and João, who gave me a huge support during this year and also a lot of motivation and help during my project, even when I was in Cardiff.

Last, but not least, I want to express my eternal gratitude to my parents and brother for their unceasing encouragement, support and attention. I am also grateful to my girlfriend, Beatriz, for her patience and strong support, especially during these times when I was abroad.

Abstract

The main objective of the work presented is the improvement of a Computer Numeric Control (CNC) automatic approach for Atomic Force Microscopy (AFM) probe-based machining. It is split in two different phases corresponding, respectively, to the improvement of the range of tip motions and the study of machining errors in function of the cutting force. In the first part, it is proposed to develop a CAD/CAM approach under LabVIEW™, which will allow an enhanced level of motion control of the stage of the AFM for performing AFM probe-based machining operations, as well as, a higher portability among different AFM instruments. Therefore, several programs in the mentioned software were developed to perform machining tasks alongside different types of complex trajectories. Specially, along curvilinear paths (Bézier curves or polynomial splines), which has not been technically feasible until now. All the programs developed in LabVIEW™ are based on parametric equations, which were improved adding motion laws to enhance its behaviour, namely in terms of smoothness.

Some studies were also performed to study a way to translate the numeric signal generated by LabVIEW™ into an analog signal, readable by the nanopositioning table, in Lille, or the AFM, in Cardiff. It was possible to do so, as well as, to send this signal to the nanotable using specific National Instruments™' devices with BNC connectors.

Then, in the second phase of this project, the AFM in Cardiff was used. The machined grooves performed with it were analysed and the data gathered with the photodiode was translated into cutting force (normal and tangential force).This allows the user to find a possible source of errors, so that it is possible to correct them by anticipation. Moreover, the obtained grooves were evaluated in terms of pile-ups formation and in terms of depth and width, according to the load applied.

Keywords AFM nanomachining, Tip path trajectories, CAD/CAM automation, Motion laws, Cutting force.

Resumo

O objetivo deste trabalho é a melhoria da automação de um processo de maquinagem CNC utilizando um Microscópio de Forças Atómicas (MFA), cuja ferramenta de remoção de material se baseia numa sonda. Este trabalho está dividido em duas fases distintas, sendo estas, a melhoria da gama de movimentos da ponta da sonda (que vai penetrar no material), e o estudo dos erros de maquinagem em função da força de corte aplicada.

Na primeira parte deste estudo, é desenvolvida uma abordagem CAD/CAM usando o *software* LabVIEW™, que permitirá obter um maior nível de controlo sobre o MFA para a realização de tarefas de maquinagem, bem como uma maior portabilidade entre os diferentes instrumentos de forças atómicas existentes. Deste modo, foram realizados vários programas para efetuar trajetórias complexas, em LabVIEW™, especialmente, segundo trajetórias curvilíneas (curvas de Bézier ou curvas polinomiais definidas por dois ou mais nós), o que não tinha sido possível realizar até então. Todos os programas desenvolvidos no *software* já mencionado são baseados em equações paramétricas, sendo melhorados introduzindo leis de movimento para aperfeiçoar o comportamento do MFA durante a maquinagem, nomeadamente em termos da suavidade do movimento.

Foram realizados alguns estudos para permitir fazer a conversão do sinal numérico geral pelo LabVIEW™, para sinal analógico, lido pela mesa nanométrica, em Lille, ou pelo MFA, em Cardiff. Tal tarefa foi possível de concretizar, bem como o envio deste sinal para a mesa nanométrica, usando alguns dispositivos da National Instruments™ com ligações BNC.

Na segunda fase deste projeto foi utilizado o MFA, em Cardiff, foram concretizadas simples tarefas de maquinagem (pequenos sulcos), que posteriormente foram analisados. Os dados do processo de maquinagem recolhidos com a ajuda do foto-díodo permitiram mais tarde, calcular a força de corte (normal e tangencial). Esta possibilidade revela-se crucial neste estudo, uma vez que poderá ser possível descobrir uma possível fonte de erros relacionada com estas forças envolvidas no processo de corte e, assim, corrigi-los antecipadamente. Além do que foi acima descrito, os sulcos realizados foram também

avaliados em termos da quantidade de material removido, da sua profundidade e largura, relativamente à carga inicialmente aplicada.

Palavras-chave: Nanomaquinagem, Microscópio de Forças Atómicas, Automação CAD/CAM, Leis de movimento, Força de corte.

CONTENTS

LIST OF FIGURES

LIST OF TABLES

SIMBOLOGY AND ACRONYMS

Simbology

x ( ) – Position coordinate according to the x-axis;

y ( ) – Position coordinate according to the y-axis;

$\dot{x}$ ( ) – Velocity according to the x-axis;

$\dot{y}$ ( ) – Velocity according to the y-axis;

t – Time variable;

t_f – Displacement time/duration;

F_t – Tangential Force;

F_n – Normal Force;

$V_{A\text{-}B}$ – Voltage A-B (corresponding to photodiode output signal, related to the cantilever's deflection);

$V_{C\text{-}D}$ – Voltage C-D (corresponding to photodiode output signal, related to the cantilever's torsion);

α, β – Calibration parameters;

φ – The angle of the cantilever, in relation to the machining surface

K_N – Normal spring constant of the cantilever;

S_N – Normal sensitivity of the cantilever;

L –The set point force;

A – Adhesion force

θ – Calibration sample slope's angle

μ_w – Friction coefficient

Ms, Mf, ms, mf – Average of the voltage related to the calibration sample

W_{slope} – Half-width of the sloped surface (of the calibration sample)

W_{flat} – Half-width of the flat surface (of the calibration sample)

Δ_{slope} – Offset of the sloped surface (of the calibration sample)

Δ_{flat} – Offset of the flat surface (of the calibration sample)

Acronyms

AFM – Atomic Force Microscope

BNC (cable) – Bayonet Neill-Concelman (cable)

CAD/CAM – Computer-Aided Design/Computer-Aided Manufacturing

CV – Coefficient of Variation

CNC – Computer Numerical Control

DAQ (module) – Data-Acquisition (module)

ENSAM – École Nationale Supérieure d'Arts et Métiers

FD – Force-Displacement

FPGA – Field Programmable Gate Array

LAO – Local Anodic Oxidation

NI™ – National Instruments™

OP-AMP – Operational Amplifier

PS™ – Park Systems™

PSPD – Position Sensitive Photo Detector

SAM – Signal Access Module

SPM – Scanning Probe Microscopy

STM – Scanning Tunnelling Microscope

VI (LabVIEW™) – Virtual Instrument (LabVIEW™)

1. INTRODUCTION

1.1. State of the Art

1.1.1. The Atomic Force Microscope

Since the invention of the Atomic Force Microscope – AFM – (it is part of the microscopy branch of Scanning Probe Microscopy (SPM)) a whole new range of measurement capabilities appeared. The SPM was created after the invention of the Scanning Tunnelling Microscope (STM), which uses a tunnelling current between a probe tip and a sample in a vacuum state to measure the surface topography. Thus, the AFM is considered as the third generation microscope (Corporation, 2010), which supports its users to go deeper into the nanoscale world.

The Atomic Force Microscope was initially designed for imaging and characterization purposes. Its primary scope is the measurement of ultra-small efforts on very small particles, such as atoms (Binnig & Quate, Atomic Force Microscope, 1986). The device has also the capability of moving controllably these atoms (Eigler & Schweizer, 1990). In this work, a considerable number of neon atoms were dispersed in a nickel surface and they were then re-arranged in order to set a patterned array. These were one of the vast capabilities of the AFM recognized some years ago.

From that time on, the Atomic Force Microscope is being even more used for other purposes. Since the early 90s, this tool is being used for machining purposes. On their first experimentations, (Jung, et al., 1992) were able to perform indentations, lines and other complex patterns with three different techniques (indentation, ploughing and dynamic ploughing – see Figure 1.1), using the AFM. They ended up concluding that the most important aspect in their experiments (and probably in many others using the AFM) was the careful control of the force of the cantilever, which had to be previously calibrated. Also, the minimization of the wear effect should be taken in consideration. This article is of great importance, since it divulges the beginning of machining tasks with this type of tool.

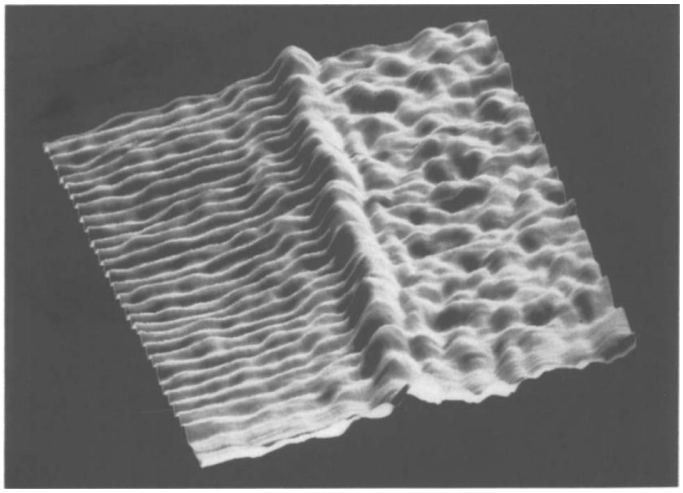

Figure 1.1 Example of a ploughing modification after the first experiments in machining in the AFM [extracted from **(Jung, et al., 1992)**].

1.1.2. Computer Aided Design/Computer Aided Manufacturing (CAD/CAM) developments

Nowadays, more and more companies bet on the development of CAD/CAM software with several different capabilities, which are related to their high level of automation. The automation can have a really important role, since it can shorten the manufacturing of several machining tasks. With the increasing complexity of components it is of great importance to reduce their global cost, in what concerns efficiency and quality. However, as seen above the users of this type of software may ensure that their system can cope with the majority of its CAD/CAM project. This is to say, that the software should be as flexible as possible, that is to say, with a high level of portability/automation.

There are several machining techniques of machining using the AFM. They are realized on it, after the pattern is drawn using a CAD/CAM software. These techniques are commonly called **nanolithography**, and they can be split in some sub-categories, such as **scratching** (material removal) or **anodization** – these are the two most important and recognized techniques. There are several important articles where CAD/CAM approaches were developed to realize the desired patterns using this type of pattern drawing. Some studies will be detailed in the following sections.

1.1.2.1. Material removal – scratching

In 2010, (Brousseau, et al., Microscopy Scratching for Small and Medium Series Production of Polymer Nanostructured Components , 2010) developed a low-cost master

making technology (small and medium series), for the fabrication of nanostructured polymer components. The authors studied the effect of different scratching parameters on the obtained surface roughness and depth was accomplished. In their work, the authors prepared a silicon sample using wire electrodischarge, which was then coated. A mask was applied, as well. Moreover, it is worth saying that a particular coated area where the scratching operations would be performed was selected, in order to more easily find the machined patterns during the going-over steps. The scratching technique was executed using standard noncontact cantilevers (due to its constant nominal force of 42 N/m – higher stiffness) and the calibration of the force applied by the cantilever was done by recording force-distance curves and then using the force constant given by the producer. However, due to the thickness of the cantilever some uncertainties might have appeared in the computed force. Nonetheless, those uncertainties could be neglected for the research in question.

For the present study the practicability of a replication by microinjection moulding was tested. To act in accordance with the constrictions and moulding requirements, a secondary mould insert was used and modified to lodge the silicon sample, as depicted in Figure 1.2.

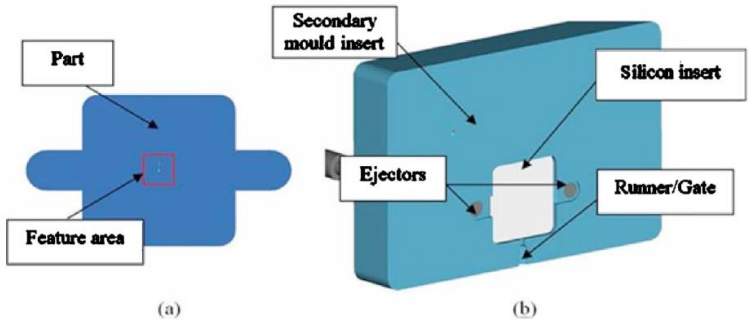

Figure 1.2 Part design (a) and insert assembly (b) [extracted from **(Brousseau, et al., Microscopy Scratching for Small and Medium Series Production of Polymer Nanostructured Components , 2010)**].

The chosen material to conduct the replication tests was polypropylene and the pattern to be replicated was the Siemens star. Because silicon is more suitable for prototyping purposes, another AFM scratching experimental was conducted on brass, which is more appropriate as a master material for microinjection moulding.

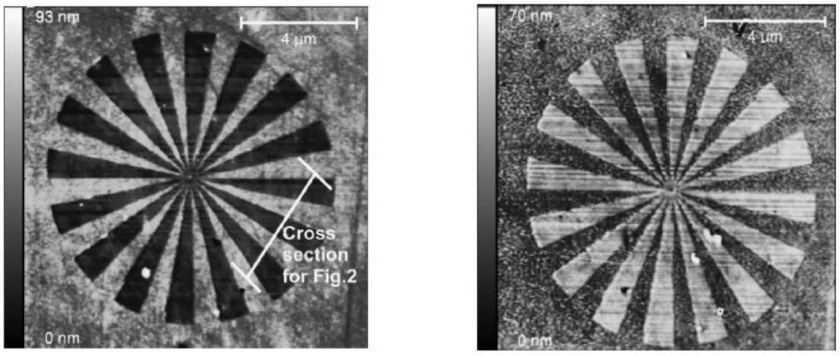

Figure 1.3 Master structure and its replication in polypropylene [extracted from **(Brousseau, et al., Microscopy Scratching for Small and Medium Series Production of Polymer Nanostructured Components , 2010)**].

Therefore, all the experimentations needed were carried out (the scratching experiments were made on grains corresponding to the brass's α phase). The master structure was machined using the raster-scanning technique (see Figure 1.3). Four scratching parameters were selected to investigate their influence on the process: applied force; scratching speed; number of cycles; step-over. The authors concluded that the parameter with the highest influence on the obtainable surface roughness and depth was the step-over. The obtained results are really important, since this parameter may be considered as the most important one in many scratching tests, in order to get good results. Moreover, this technique is very likely to be used widely for the fabrication of nanostructured replication masters (for small to medium series production).

1.1.2.2. **Anodization**

This pattern-fabrication technique consists in a procedure where, through an electrolytic process, the thickness of a metal part is increased, by means of an oxidation (creation of a local oxide layer) process.

Although this method could be included in the nanolithography section, since most of the anodization approaches rely on nanolithographic abilities, it was decided to consider it separately, due to the relevance of such studies, performed by Johannes et al.

Therefore, in 2006, (Johannes M. S., Kuniholm, Cole, & Clark, 2006) tried to associate the design capabilities of CAD/CAM software with the strengths of AFM's nanolithography.

The chosen pattern (in this case, the characters "D", "U", "K", "E") was drawn using a proper CAD software (SolidWorks™) and the generated file was converted to G-

code using specific software for a purpose like this. This G-code language (which is commonly used in Computer Numeric Control platforms) is particular interesting since it contains all the fabrication parameters of the pattern to be machined and all the coordinates of the machining points, as well as all the indispensable knowledge to generate movement commands for the AFM system.

Moreover, the great benefit of this type of files lies on the fact that it is possible to shape it accordingly to our design specifications through proper programming procedures.

In order to have a better handling of the tip progression a proportional-integral controller was introduced, which also allows the system to have independent feedback control loops on each axis.

Consequently, the first anodization lithography process was made (see Figure 1.4). The sample used was a silicon wafer and the machining parameters were chosen due to their suitability in what concerns the aspect ratios of the attained pattern. Thus, the parameters used were: force setpoint of 1 nN, tip writing speed set to 1 μm/s and bias voltage equal to 8 V.

Figure 1.4 AFM image of the obtained pattern [extracted from **(Johannes M. S., Kuniholm, Cole, & Clark, 2006)**].

Finally, to test the capabilities of the system in cause another study with a more complex pattern (several connected arcs and semicircles) was imaged. The obtained results can be seen on Figure 1.5.

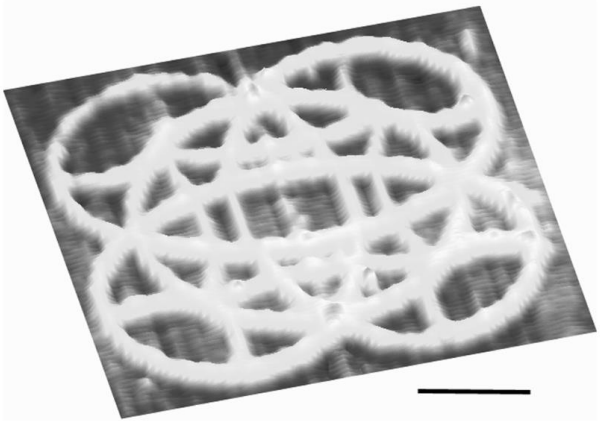

Figure 1.5 Image of the complex pattern obtained after ANL [extracted from **(Johannes M. S., Kuniholm, Cole, & Clark, 2006)**].

One year later, in 2007, (Johannes, Cole, & Clark, Three-dimensional design and replication of silicon oxide nanostructures using an atomic force microscope , 2007) used the same method and procedures (generation of a G-code file - it contains vector scanning information - which was used together with the AFM nanolithographic capabilities), but they decided to machine 3D patterns. One of the new implementations used was the self-prescription of bias voltage and tip velocities according to the desired feature height, by the system.

For this specific case where a 3D pattern is meant to be drawn in a silicon wafer using Local Anodic Oxidation (LAO), it is important to note that a careful control of the voltage bias will have a linear impact on the oxide height with all the other relevant parameters for the study in question: speed, humidity and force. It was also possible to prove that, keeping speed, voltage and force constant relative humidity disturbs the oxide line width. These studies were important since they allowed the authors to explain in which way both environmental and experimental parameters affect the formation of silicon oxide structures.

Another important aspect that should be kept in mind on this family of studies like this is the calibration step that shall always be made when working with this type of techniques. In this case, several errors appeared due to the association between the oxide width and bias voltage.

After testing the behaviour of the whole system (AFM-sample) under different conditions and altering the parameters involved, previously mentioned, the 3D structures were then replicated.

Several tests were then performed. In the first one, four 3D structures with increasing height were made and then multi-height silicon oxide constructions were created, as well.

Finally, and certainly the most important test was performed. A circle, a triangle and a star were built. The singularity of this test lie on the fact that they have a critical lateral dimension of 500 nm, which can cause some problems during LAO.

One of the main drawbacks that the authors faced when performing patterns like these ones, had to do with the G-code interpreter, because it was incapable of assigning proper coordinates to fill in the vertices of the triangle. An important finding of this work is related to the fact that there are some significant discrepancies between the predicted height of replicated nanoscale structures and actual feature heights on the order of the AFM sensing limits. The results of this latter test are depicted on Figure 1.6.

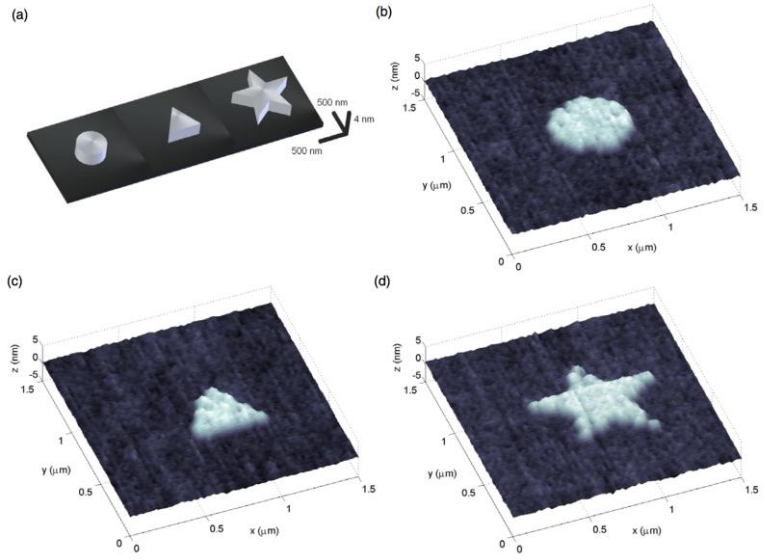

Figure 1.6 (a) CAD design of the desired shapes; (b)-(d) contact AFM height images of the obtained structures [extracted from **(Johannes, Cole, & Clark, Three-dimensional design and replication of silicon oxide nanostructures using an atomic force microscope , 2007)**].

2. THE ATOMIC FORCE MICROSCOPE ITSELF: A POWERFUL AND FLEXIBLE TOOL

2.1. Context

Nanotechnology is nowadays undergoing an emerging process. Due to its development in the last years, it is now a very recognized field of research, and a really promising science for the near feature, with possible applications in the manufacturing of several products in many different areas. This recent research field carries really interesting challenges not only for researchers but also for engineers. On the other hand, the appearance of new materials with very appealing properties plays a very important role on the development of nanotechnology.

The Atomic Force Microscope (AFM) is a decisive tool for the development of nanotechnology. This precision tool was created in 1986 (Binnig & Quate, Atomic Force Microscope, 1986) and it is a technique of Scanning Probe Microscopy (SPM), which covers several related technologies for imaging and measuring surfaces on a fine scale, down to the level of molecules and groups of atoms.

The AFM has several advantages, since it allows the measurement of non-conducting materials and permits also to characterize soft samples, such as biological specimens.

Thus, nowadays, scratching techniques are also possible to perform using this tool. It is under this technique that this project will rely on, in order to confirm the feasibility of using a software, such as LabVIEW™, to enhance the freedom of motion of the AFM.

It is important to note that this work is not a CAD/CAM project, since its main objective is not the development of a software, but to obtain an efficient machining at nano-scale by a freely range of motion and with a high level of automation, with the help of, LabVIEW™ program. Nevertheless, this project establishes a first step towards achieving a fully automated CAD/CAM process.

2.2. AFM parts

This tool is a 3-axis system (X, Y, Z) composed by a nanometric table, which allows displacements along X, and Y-axis for the sample, and a tip-lever system triggered

by a piezoelectric actuator, which moves along the Z-axis (Binnig & Quate, Atomic Force Microscope, 1986), as it can be seen on Figure 2.1. Basically, this instrument is no more than an imaging system at micro/nanometric scale; by default, the X and Y displacements are used for scanning strategies. Thanks to the feedback control of the Z-axis, through the measurement of the lever deflection by means of a photodiode and by exploiting the forces of attraction/repulsion between the atoms of the tip and the model, it is possible to determine the sample's topography. In non-contact mode, these variations of attractive and repulsive forces, allow the user to measure the efforts applied by the cantilever and thus, establish the sample's topography (3D image).

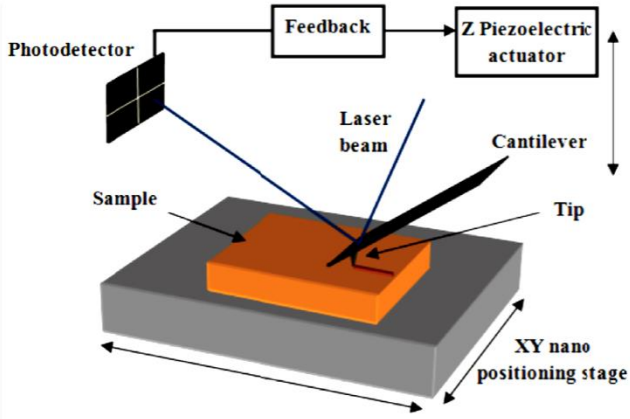

Figure 2.1 Atomic Force Microscope working principle [extracted from **(Brousseau, et al., 2013)**].

The displacement of the Z-axis using the photodiode is used to control the force of the cantilever and, therefore, the deflection of the lever. Moreover, the force applied to the sample will determine the depth of the cut.

More recently, the nanometric table is being used as a tool to perform several nano fabrication tasks, for instance, it is used as a machining tool, whether for deposition (Cruchon-Dupeyrat, Porthun, & Liu, 2001) and (Horcas, et al., 2007), whether for removal of material (see section 1.1.2.1)**.**

The brand that produces this equipment – Park Systems™ (PS™) – offers several software to perform really simple nanolithographic patterns using the AFM (see section 4.1). However, these solutions provided by this AFM manufacturer are really limited, especially in what concerns:

- The range of tip motions that can be developed (really simples trajectories, with a slope equal to 1);

– The flexibility in performing desired defined tip displacement strategies;
– The portability, in order to easily transfer tip trajectories data between different AFM instruments (for example, the solution created by the software of PS™ can only be used in AFM manufactured by PS™), which will cause a big lack of automation.

2.3. CAD/CAM approach developed in the context of this project

A first CAD/CAM approach has already been developed with the purpose of moving the table along more complex trajectories rather than a scanning strategy (default strategy), and with a high level of automation (Johannes M. S., Kuniholm, Cole, & Clark, 2006). (Brousseau, et al., 2013), in his work, from the pattern drawn under the CAD/CAM software generated a G-Code file, which is not readable by the AFM controller. A post-processor is then used (in C++ language) to translate the G-Code file into instructions readable by the AFM controller (a scheme of the process is depicted on Figure 2.2a).

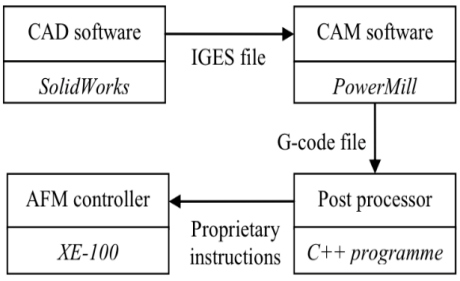

Figure 2.2a CAD/CAM approach used [extracted from **(Brousseau, et al., 2013)**].

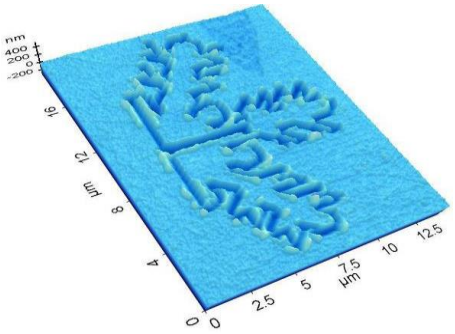

Figure 2.2b Machining of a half snowflake with the CAD/CAM approach [extracted **from (Brousseau, et al., 2013)].**

Although this approach has proven to be successful (Figures 2.2a and 2.2b), it was only possible to control one input voltage of the nanometric table: either one single voltage to move the table along the X-axis or Y-axis or the exact same voltage to move both axis (slope equal to – or + 1). Due to this limitation of the table motion, the pattern was segmented using Bresenham's algorithm according to segments oriented along the possible displacements. For instance, Figure 2.3, illustrates the segmentation of a straight line with a slope different than – or + 1. Some unwanted features emerged. They are related to the interruption of the tip progression during machining, which has an effect on the surface

quality at the bottom of the produced grooves and also generates the appearance of excessive amounts of pile-ups along the whole path (Figure 2.4).

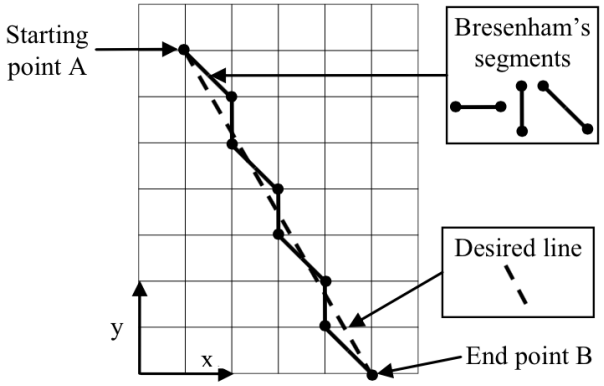

Figure 2.3 Bresenham's Line Algorithm.

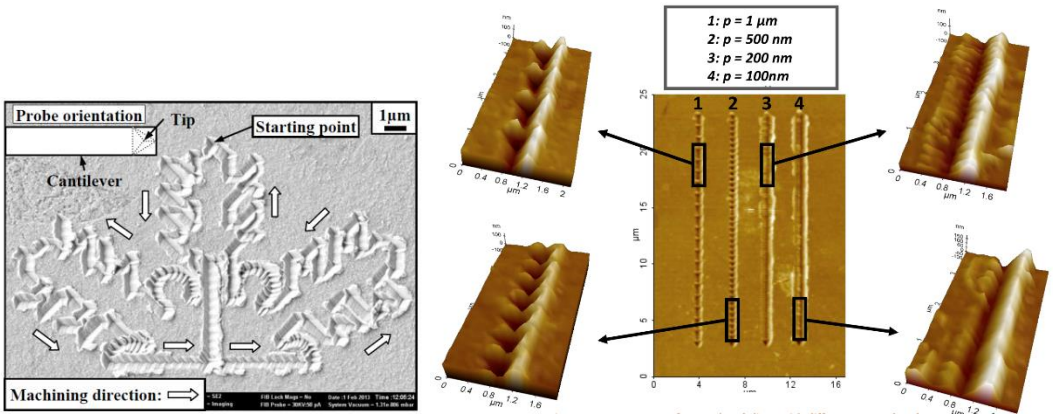

Figure 2.4 Unwanted features – interruption of the tip progression and accumulation of pile-ups.

The present project will be made with the purpose of improving this CNC automation approach using National Instruments™ equipment in order to avoid the emerging unwanted features. Indeed, with this new equipment, a recent study (Michaut & Rozier, 2014/2015) has shown the feasibility of sending two different voltages to a X-Y nano-positioning table, allowing for a freedom of motion, by integrating FPGA programming. This is not really desirable due to the complexity of such approach.

The main aim of the current project is to study the integration of a LabVIEW™ solution on Cardiff's AFM and, thus, to conduct experiments of machining along straight lines with a slope different than – or + 1 and also along Bézier's Curves, which allows to perform much more complex trajectories, such as curvilinear ones.

2.4. Thesis' approach

Before proceeding with the description of the main purpose of this thesis, it is extremely relevant to present the approach that is the basis of this project, depicted on Figure 2.5.

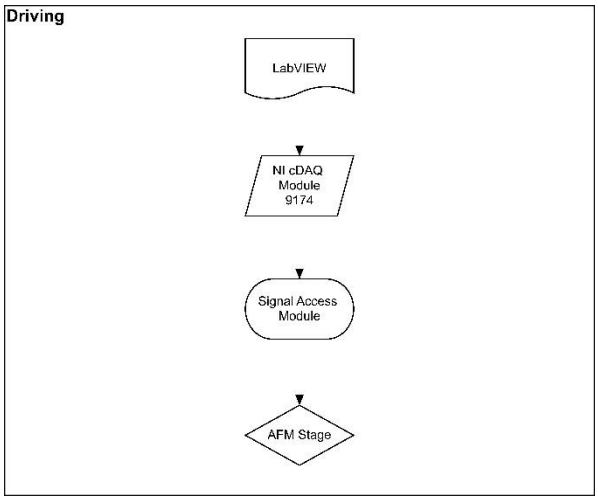

Figure 2.5 Thesis general approach diagram.

The main objective of the project is the driving of the AFM stage using LabVIEW™ (it allow sending 2 separate voltages to each axis). However, between each equipment, there are others, not less important devices, such as the National Instruments cDAQ 9174 module (where the card NI 9223 is plugged to acquire the signal provided by the AFM's photodiode) and the Park Systems Signal Access Module (Figure 2.6). Therefore, the information sent by the computer (with LabVIEW™) flows through each stage, till reaching the AFM where the desired task is performed.

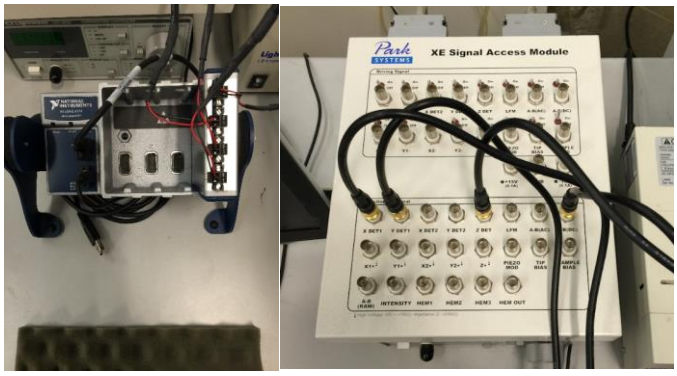

Figure 2.6 Pictures of the cDAQ Module 9174 and the Signal Access Module.

2.5. Work planning

The following work will be developed throughout this project:

1. Development of several programs with LabVIEW™, in order to control the nano-positioning table and, thus, to improve its freedom of motion; then, after this step, the control of the nanometric table should only be improved using the LabVIEW™ software – these tests will be developed in the laboratories of ENSAM Lille; the different tests will be performed in the following order:
    - Straight lines trajectories with parametric equations with time discretization;
    - Straight line trajectories with a cubic law equation – to have a more smoother plan trajectory;
    - Two consecutive straight lines – they have a different slope, which will make the machining direction to change;
    - Curvilinear trajectories with Cubic Bézier's Curves – they actually have a smooth behaviour – with the possibility of adapting the speed by changing the displacement time, t_f.
    - Circle – in order to have a complete rounded trajectory;
2. Implementation of the work above described on Cardiff's AFM and performance of experimental studies to evaluate several aspects regarding the obtained patterns, such as:
    - Efficiency – accuracy of the trajectory tracking;
    - Quality – roughness and height profile;

Subsequently, through the experimental tests, the tip path trajectory should suffer some corrections by anticipation (if possible, an error pattern should be found out). These experimental tests will be performed in Cardiff University.

2.6. Constraints found

As mentioned in section 0, there are several devices that are part of the machining process. They help to translate the data that flows from its very beginning till the conclusion of the wanted pattern.

The software with which this project is developed, LabVIEW™, generates a numeric signal, which is not readable by the SAM. All the connections made between the custom equipment, such as the cDAQ 9174 module and the SAM, are done using a BNC cable (Bayonet Neill-Concelman), which is only capable of transferring analog signal towards the SAM. Thus, in order to convert the numeric signal into analog signal a module from National Instruments was tested – NI Module 9269 (see Figure 2.7).

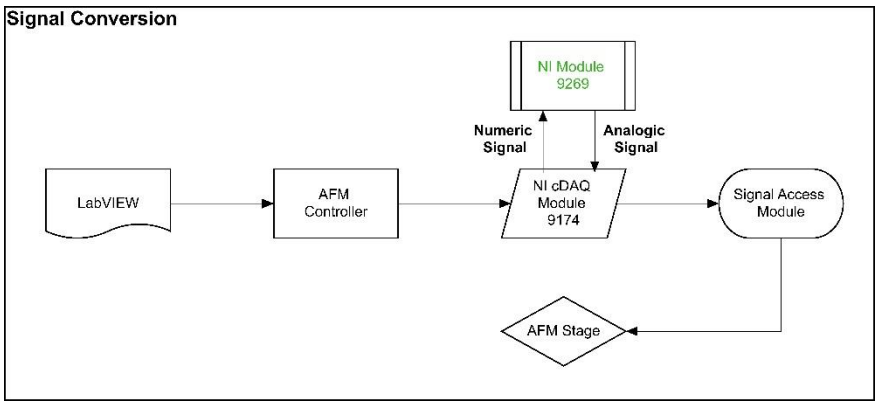

Figure 2.7 Signal Conversion Diagram.

However, one important aspect that should be taken into consideration, concerning this signal conversion, is the technical characteristics of the conversion equipment (NI Module 9269) and the SAM, shown in Table 2-1:

Table 2-1 Technical characteristics of the SAM and the conversion module.

Technical Characteristics		
	Signal Access Module by Park Systems	**National Instruments Module 9269**
Resolution	-	16 bits
Maximum Voltage	24 V	10 V
Voltage Range	0 to 10 V	-10 to 10 V
Current Drive Single	-	0,01 A
Current Drive All	-	0,02 A
Hold Current	0,025 A	-
Trip Current (where the device interrupts current)	0,085 A	-
Impedance	33 Ω	0,1 Ω

As it is visible on Table 2-1, the impedances of each equipment are different (33Ω vs. 0,1Ω), which means that, in this case, the module 9269 cannot supply enough power to the Signal Access Module. This will make the task of machining impossible to accomplish, since the x and y axis of the AFM stage cannot even make any displacement.

2.6.1. Unlocking the constraint

2.6.1.1. Operational Amplifier

In order to overcome the problem that has arisen, a solution able to increase the power supplied to the SAM was necessary to be found. A possible answer (though not tested during the development of this project) can be the utilization of a little device called Operational Amplifier (Figure 2.8).

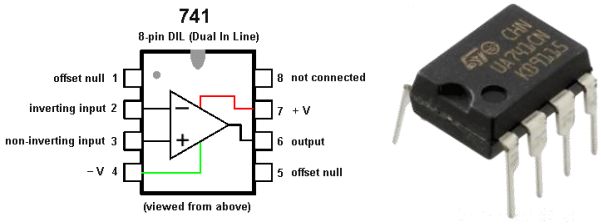

Figure 2.8 741 Op-Amp connections (left) and its appearance (right).

This instrument is nothing more than a high-gain DC coupled amplifier with two inputs (2 and 3) and only one output (6). The more recent version of this device has an

integrated circuit and it is named "741 operational amplifier". Basically, the DAQ module should be, somehow, plugged in the input connector (2) and the output of the op-amp (6) should be connected to the SAM. The input (3) is the grounded connection.

Another solution that can unlock this situation is to use a PXI controller (this solution was tested and with it, it is possible to perform displacements in Lille's nanotable (see section 2.6.1.2), which is linked to our LabVIEW™ software, instead of using the NI-cDAQ module.

2.6.1.2. **PXI controller working principle**

The PXI controller (Figure 2.9) was tested in Lille, in order to see whether it was possible or not to connect it to the nanopositioning table's controller and, thus, displace the table, using the LabVIEW™ programs made before.

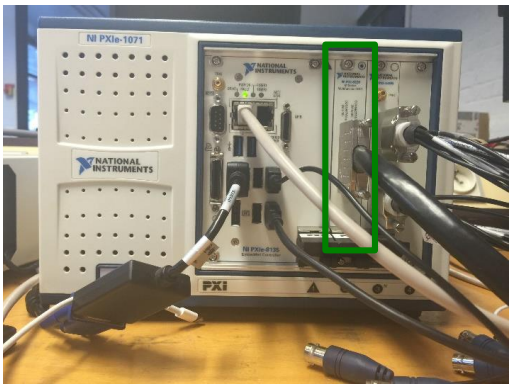

Figure 2.9 NI PXIe-1071 Chassis and NI-PXI 6229 card (green).

However, let's first understand in which way all these devices are connected between them, with the help of Figure 2.10.

Figure 2.10 Scheme of the data flowing process between LabVIEW and the table's controller.

As it can be seen, the LabVIEW™ software is installed in the 4 slot-NI PXIe-1071, which has the NI PXI-6229 installed on it (inserted on PXI-e 1071's second slot – green coloured). Then, the Virtual Instrument (VI) created in LabVIEW™ is able to generate a numeric signal that will be converted to analog signal by the 6229 card, since this is the only type of signal that the nanopositioning table's controller can read. Finally, there is the

connection block SCB-68A, which is used for connection purposes, since it has several BNC connectors, plugged in the table's controller. It was decided to test this device, due to its high impedance, which allows it to be coupled with the Signal Access Module.

2.6.1.3. Signal generation

In order to verify if everything was working properly, the output connectors were plugged into an oscilloscope, to see if any type of analog signal could be generated. A picture of all the devices is shown on Figure 2.11.

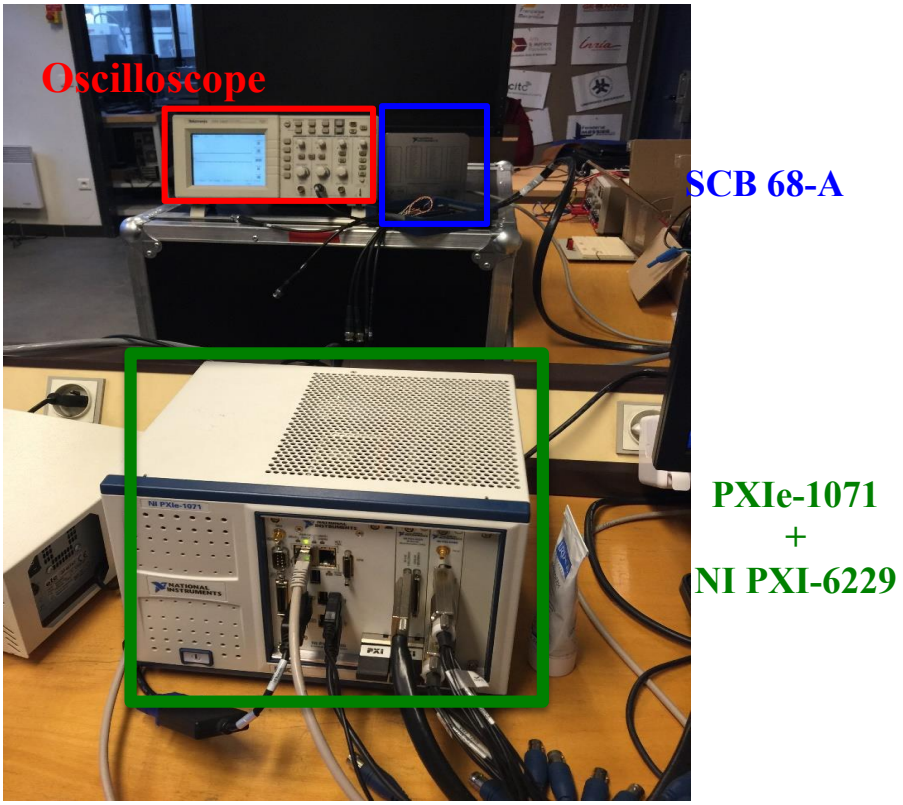

Figure 2.11 Line-up of all the devices needed to generate an output voltage.

With this setup, it was possible to send a signal to the oscilloscope, but before doing so, some problems arised, to find out the correct output connectors. Thus, some cautions need to be taken when connecting the block SCB-68A to the oscilloscope because it has BNC connectors that are used for acquisition and generation purposes (Figure 2.12).

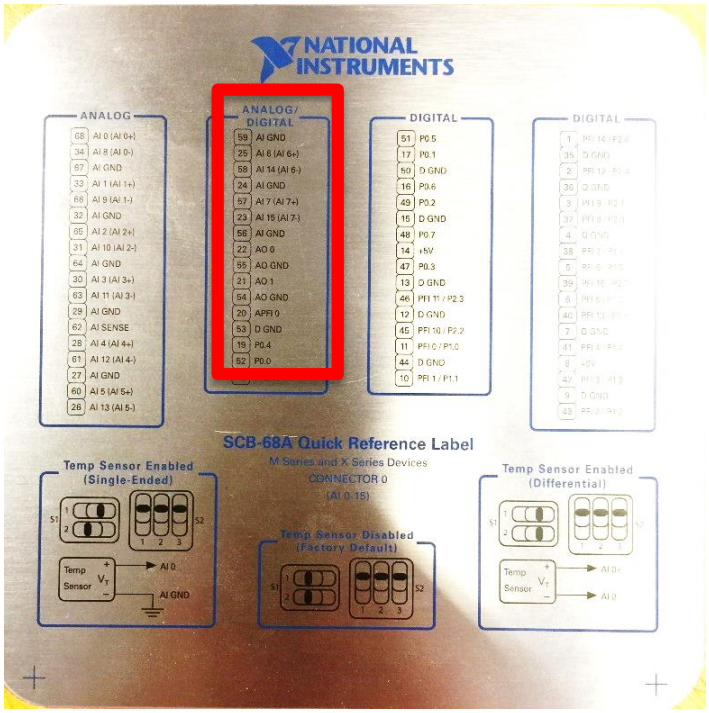

Figure 2.12 SCB-68A covering plate with all the information's about the input and outputs.

The outputs that need to be used are those that are associated to the pin's description. They can be seen inside the red rectangle.

Moreover, the Virtual Instrument (VI, on LabVIEW™) designed to send an analog signal to the oscilloscope is presented on Figure 2.13.

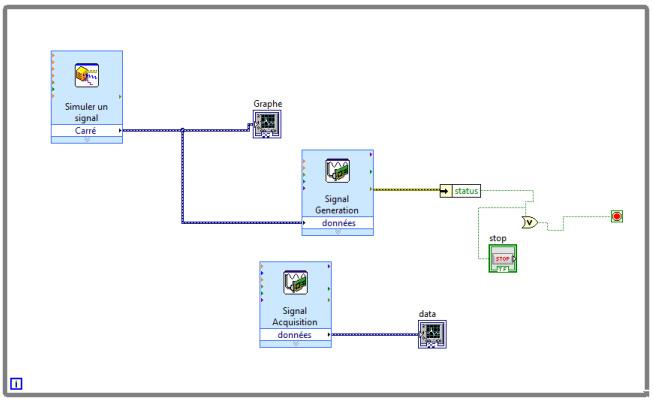

Figure 2.13 Block Diagram interface of the program for signal generation.

When drawing this VI the only aspect that must be carefully treated, was the configuration of the DAQ Assistant for both the Signal Generation and Acquisition, because the outputs designation needs to be in concordance to the block SCB 68-A.

2.6.1.4. **Signal acquisition**

In order to acquire the signal generated, in this case, by a voltage generator, it is possible to create a DAQ Assistant for signal acquisition purposes, instead of for signal generation. In the DAQ Assistant menu the right information just needs to be inserted in the program, so that is creates an acquisition program.

This functionality was tested in Lille. The program is very simple, since it only requires that the DAQ Assistant is configured for signal acquisition purposes.

An image of all the devices connected between them is also shown on Figure 2.14.

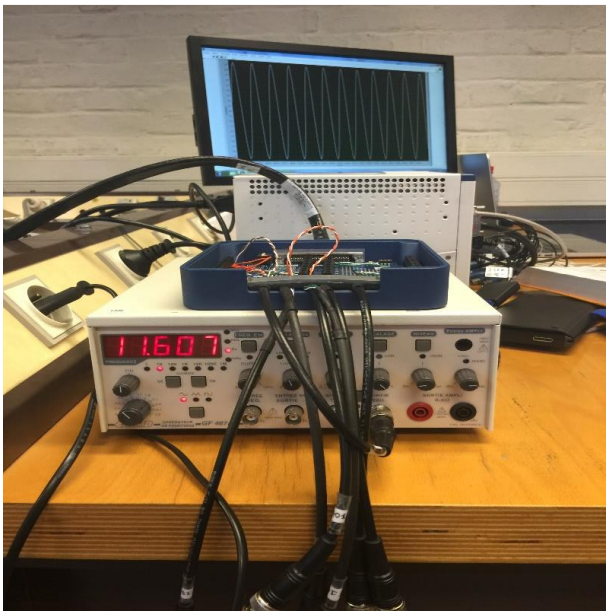

Figure 2.14 Line-up of all the devices needed to acquire a signal.

On the image above it is possible to see the sinusoidal wave generated by the voltage generator.

2.7. Objectives redefinition

Due to the problem of the lack of power between the NI Module 9269 and the Signal Access Module the objectives that were firstly defined, had to be remade. Hence:

- Instead of driving the AFM stage, in Cardiff, using the LabVIEW™ programs previously made, it was decided to perform simple straight grooves, in order to evaluate its depth and width and the pile-ups formation, as well, according to the application of different loads and machining directions – this task was done in Cardiff's AFM;

- Moreover, since the signal sent to the AFM stage is a voltage, it might be useful to translate it into cutting force because the errors that may appear can be related with this cutting force – this task was done in Cardiff;
- Finally, the programs made in LabVIEW™ were tested in Lille's nanopositioning table, in order to check the feasibility of using LabVIEW™ for CAD/CAM purposes, which unlocked the problem of sending only 1 voltage to the axis, enabling the user to send 2 voltages at the same time – this task was done in Lille.

3. LABVIEW™ PROGRAMMING

3.1. Some preliminary considerations

Before proceeding with the description of all the LabVIEW™ programs developed to test whether it is suitable to use this type of software for CAD/CAM approaches, some considerations regarding the physical differences between this software and the AFM (in Cardiff) and the nanopositioning table (in Lille), need to be made.

First of all, this software generates a numeric signal, which will need to be converted in analog signal, since the AFM controller is only able to deal with this type of signal (see section 2.4)

Secondly, and probably the most important aspect to understand in all the LabVIEW™ programs developed in this section, is that all the voltages in X and Y (they have a range from 0 to 10) will correspond to a position (for axis X and Y) in each equipment (each one has a different range of displacement). This means that, whenever someone wants to draw a straight line in a certain position, it is necessary to convert this voltage into position. Since there is a linear relationship between voltage and position, it is very easy to perform this transformation. Let's first refer the range of displacements that each instrument has:

Cardiff AFM's nanotable – [0, 45] µm

Lille's nanopositioning table – [0, 75] µm

Therefore, the value of position that wants to be obtained should be multiplied by 10 (maximum voltage allowed) and divided by 45 or 75 (the maximum displacement allowed in each instrument) – Figure 3.1.

Figure 3.1 Mechanism for getting the desired coordinates.

Let's illustrate with an example:

Coordinates: Point 1 (10; 20); Point 2 (30; 30)

Corresponding coordinates in Lille's nanopositioning table:

$$\textbf{P1: } \left(10 \times \frac{10}{75}; 20 \times \frac{10}{75}\right) = (1.33; 2.67)$$

$$\textbf{P2: } \left(30 \times \frac{10}{75}; 30 \times \frac{10}{75}\right) = (4; 4)$$

Finally, there are some physical constraints related to the velocity that were overcame by applying an adaptive duration procedure, where the speed can be controlled with the parameter t_f , which is the displacement time of the machining process(see section 3.3.2).

On a first stage, with the support of LabVIEW™ software by National Instruments, a program was developed in order to test straight lines with a slope different from 45 degrees (π/4).

The parametric equations displayed in the system (3.1) allows the user to draw a straight line:

$$\begin{cases} x(t) = (1-t)x_1 + tx_2 \\ y(t) = (1-t)y_1 + ty_2 \end{cases} \quad (3.1)$$

with $t \in [0,1]$, where $\begin{pmatrix} x_1 \\ y_1 \end{pmatrix}$ is the starting point and $\begin{pmatrix} x_2 \\ y_2 \end{pmatrix}$ is the ending point along the straight line.

The test performed is made with a time discretization, which is represented by the term ***t***.

3.2. LabVIEW™ interface

Let's give a brief explanation of the software interface, as well as its working principle.

This software is used for measurement and control purposes and two different windows compose its interface: the block diagram and the front panel. As soon as the user creates the numeric signals on the front panel menu (1 in Figure 3.4), they will appear automatically on the block diagram interface. This latter interface (as it can be seen in Figure 3.2) is used to express all the variables involved (1.1 and 1.2 in Figure 3.2), which are connected to the formulas menu 3.1. On it, it is possible to write the desired equation 3.2 that can be activated by a signal input – for instance, a triangular signal, to generate the time signal (t ∈ [0,1]) – (2, Figure 3.2 – "simulate signal"). Moreover, in 4, the connections

corresponding to the data that wants to be plotted in the graph (2 in Figure 3.4) that appear in the front panel window (Figure 3.4), need to be done.

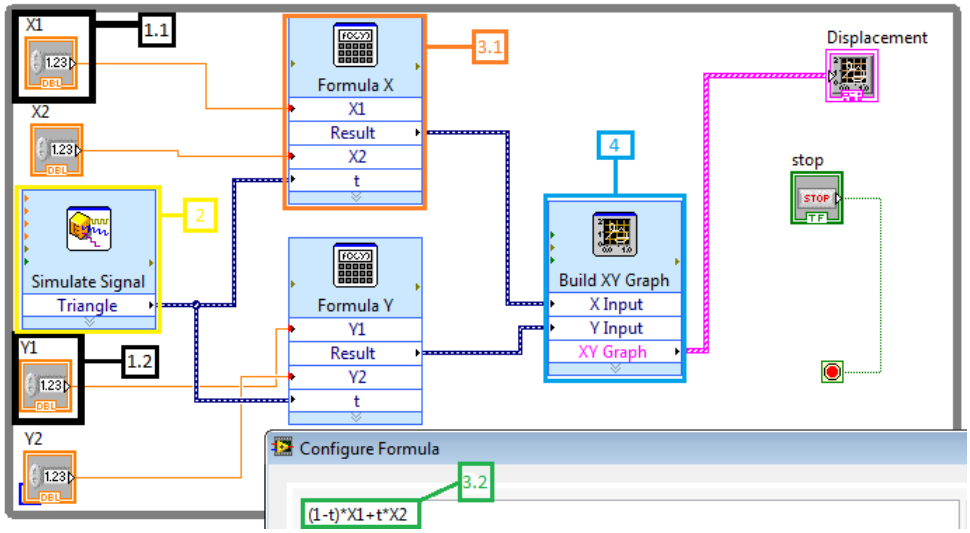

Figure 3.2 LabVIEW's block diagram interface.

3.3. Straight line trajectories

3.3.1. Single straight line

The computations that allow us to get the desired coordinates of the pattern's points in the nanopositioning table were then applied in LabVIEW™ – Figure 3.3 – (the previous image doesn't show it because this mechanism was found later).

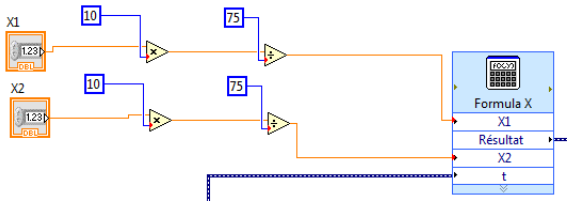

Figure 3.3 Image of the mechanism that allows to transform voltage into position in LabVIEW™.

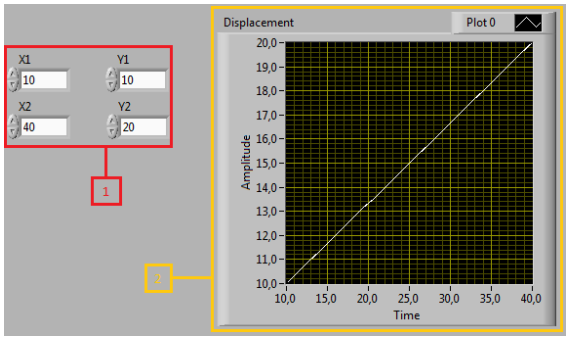

Figure 3.4 LabVIEW™'s front panel interface.

According to the program that was built (Figure 3.2 then improved with the mechanism shown in Figure 3.3) and as previously expected, the attained graph is a straight line (see Figure 3.4), which proves the feasibility of such approach, that is to say that it is possible to move the X-Y table along straight lines using LabVIEW™ software.

3.3.2. Improvement of the previous program – Smooth Approach

In order to improve the motion control of the nanometric table, since the aim is to produce the machining of straight lines, physical considerations were taken into account and, therefore, a cubical law motion was added – all the constraints represented on the system (3.2) are related with the initial, $\boldsymbol{x(0)}$, and final position, $\boldsymbol{x(t_f)}$, of the straight line and also with the initial, $\boldsymbol{\dot{x}(0)}$, and final velocity, $\boldsymbol{\dot{x}(t_f)}$, (for the y axis, the conditions are the same):

$$\begin{cases} x(0) = x_0 \; ; \; x(t_f) = x_f \\ \dot{x}(0) = 0 \; ; \; \dot{x}(t_f) = 0 \end{cases} \tag{3.2}$$

The cubic equation (3.3) was implemented to get a smoother plan trajectory:

$$x(t) = a_0 + a_1 t + a_2 t^2 + a_3 t^3 \tag{3.3}$$

and thus the respective velocity is shown on equation (3.4):

$$\dot{x}(t) = a_1 + 2a_2 t + 3a_3 t^2. \tag{3.4}$$

Replacing all the conditions shown in (3.2) on equations (3.3) and (3.4):

$$\begin{cases} x_0 = a_0 \\ x_f = a_0 + 2a_1 t_f + a_2 t_f^2 + a_3 t_f^3 \\ a_1 = 0 \\ 2a_2 t_f + 3a_3 t_f^2 = 0 \end{cases}$$

Finally, rearranging all:

$$a_0 = x_0 \; ; \; a_1 = 0 \; ; \; a_2 = \frac{3(x_f - x_0)}{t_f^2} \; ; a_3 = -\frac{2(q_f - x_0)}{t_f^3}$$

Thus, after replacing all the variables obtained above on equations (3.3) and (3.4), the following smoother equations are obtained:

$$x(t) = x_0 + \frac{3(x_f - x_0)}{t_f^2} t^2 - \frac{2(x_f - x_0)}{t_f^3} t^3 \tag{3.5}$$

$$\dot{x}(t) = \frac{6(x_f - x_0)}{t_f^2} - \frac{6(x_f - x_0)}{t_f^3} t^2 \tag{3.6}$$

The equations for $y(t)$ and $\dot{y}(t)$ are the same, but instead of x_f and x_0 we have y_f and y_0.

$$y(t) = y_0 + \frac{3(y_f - y_0)}{t_f^2} t^2 - \frac{2(y_f - y_0)}{t_f^3} t^3 \tag{3.7}$$

$$\dot{y}(t) = \frac{6(y_f - y_0)}{t_f^2} - \frac{6(y_f - y_0)}{t_f^3} t^2 \tag{3.8}$$

With these position (equations (3.5) and (3.7)) and velocity (equations (3.6) and (3.8)) equations, it is only necessary to deal with the displacement time, which is represented by $\boldsymbol{t_f}$.

Such equations are then inserted in the software (Figures 3.5 and 3.6) and the correspondent graphs are plotted as it can be seen on Figures 3.8, 3.9 and 3.10.

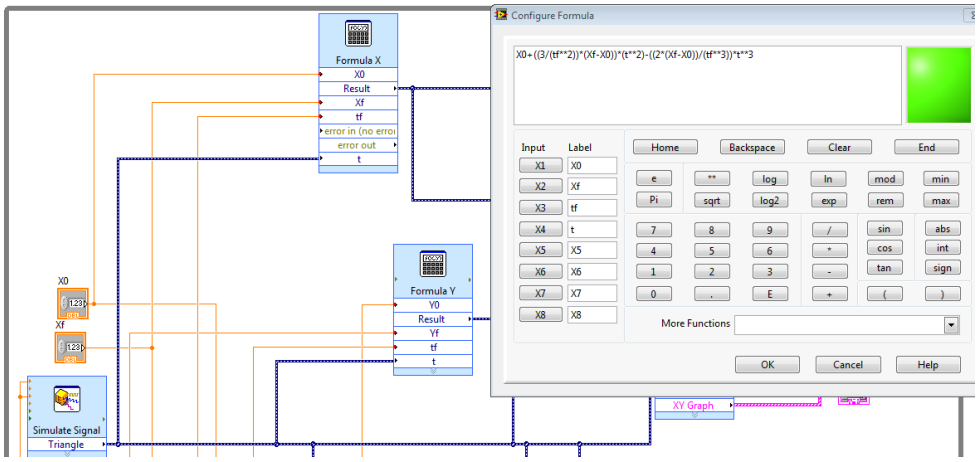

Figure 3.5 Introduction of position equations.

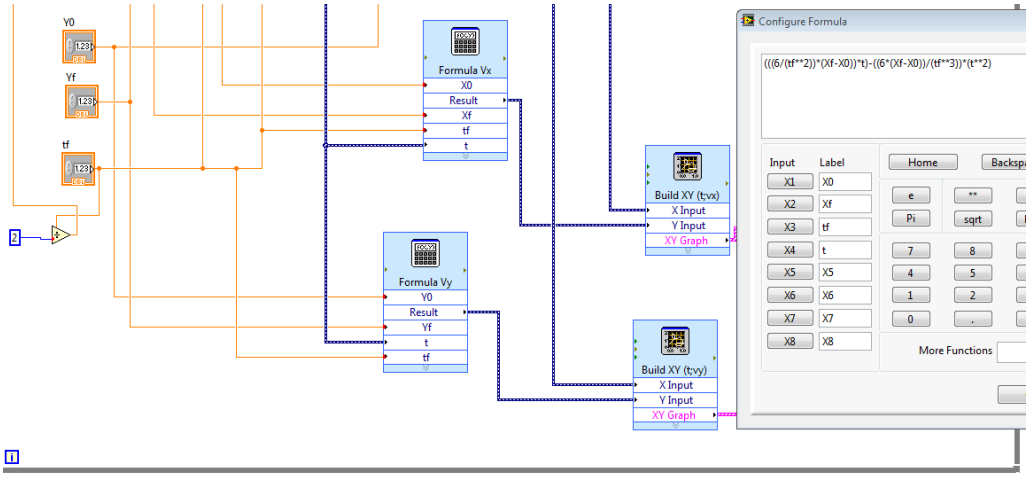

Figure 3.6 Introduction of velocity equations.

As it is shown in the block diagram windows, to generate the time signal ($t \in [0, t_f]$) a "simulate signal" block (in this case, a triangular signal) was used. However, by default, this signal takes values between [-1,1], which is not suitable for this case. Consequently, a transformation factor was applied. Its representation is depicted in Figure 3.7, and it can be numerically explained as:

$$Offset = 0{,}5 \cdot t_f$$

$$Amplitude = 0{,}5 \cdot t_f$$

$$[-1,1] \xrightarrow[\text{Amplitude}]{x\frac{tf}{2}} \left[-\frac{tf}{2}, \frac{tf}{2}\right] \xrightarrow[\text{Offset}]{+\frac{tf}{2}} [0, tf]$$

Figure 3.7 Amplitude and Offset factors.

This means that the more the displacement time is increased, the lower will be the maximum amplitude (velocity) obtained.

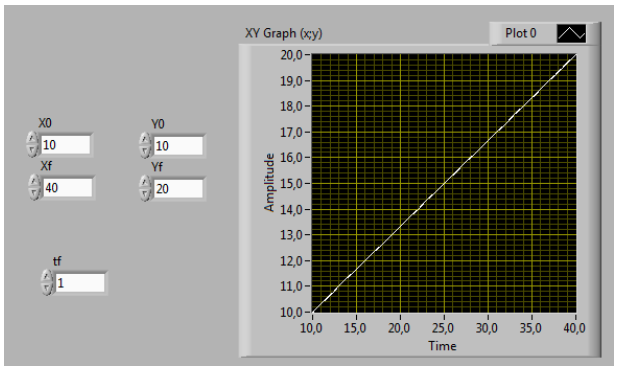

Figure 3.8 Graph of Position y(x).

The graph present in Figure 3.8 shows the trajectory performed by the tip, after linking position to voltage.

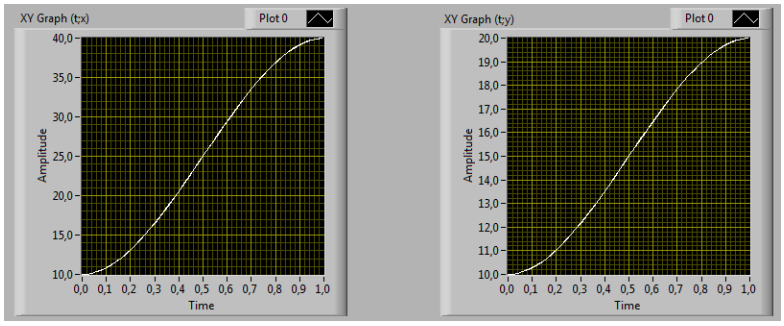

Figure 3.9 Graphs of t(x) and t(y).

Moreover, the graphs shown in Figure 3.9, allow the user to know and control the voltages sent to the table. If the reader looks carefully at them, it is visible that there are shorter displacements in the beginning and in the end, as well. This was possible after applying the cubic law motion previously mentioned.

3.3.3. **Remarks**

In order to machine more accurately, the velocity with which the task is performed should be well controlled. In fact, the velocity should be constrained since it is not desirable going too fast, otherwise the machining task is not as accurate as required.

This mechanism of controlling the speed is made by simply adjusting the duration, t_f. This allows us to have a much higher control over the AFM. The machine starts its task with null velocity, it slowly increases the speed till a maximum is reached, and then it decreases until the end of the operation.

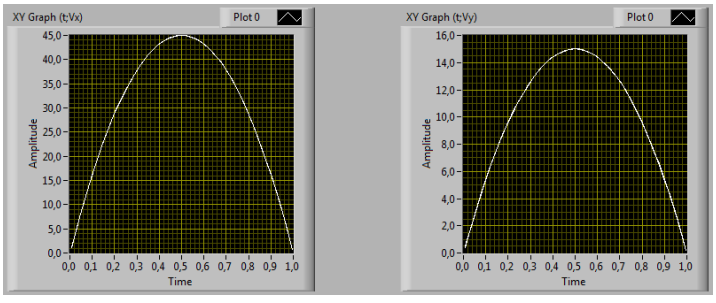

Figure 3.10 Graphs of $V_x(t)$ and $V_y(t)$.

As it was mentioned before, one of the parameters that the user is able to manipulate is the displacement time (or duration, t_f). To see the behaviour of the plotted curve, an increase of t_f from 1 to 5 was made.

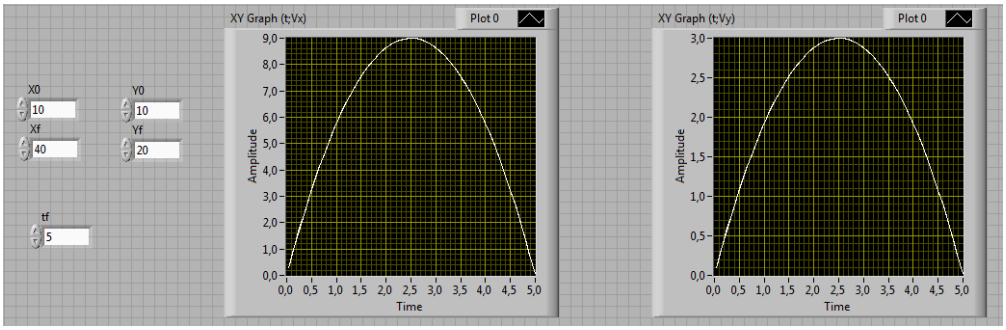

Figure 3.11 Difference on the plot after changing the time displacement.

As an increment of $5t_f$ was made, this means that the maximum reachable velocity would be $\frac{V_{max}(t_f=1)}{5} \approx \frac{45}{5} = 9\mu m.min^{-1}$ (for the first graph) – Figure 3.11 – due to the manipulation performed, as previously explained. The same is verified for the second graph, $V_y(t)$.

3.3.4. Two consecutive straight lines

After having built a program for a single straight line, it was decided to execute also a program able to perform two consecutive straight lines using parametric equations. This allows the table to change its direction during the process of scratching, and some interesting features may emerge due to this fact. Therefore, an image of the block diagram of this program is depicted on Figure 3.12.

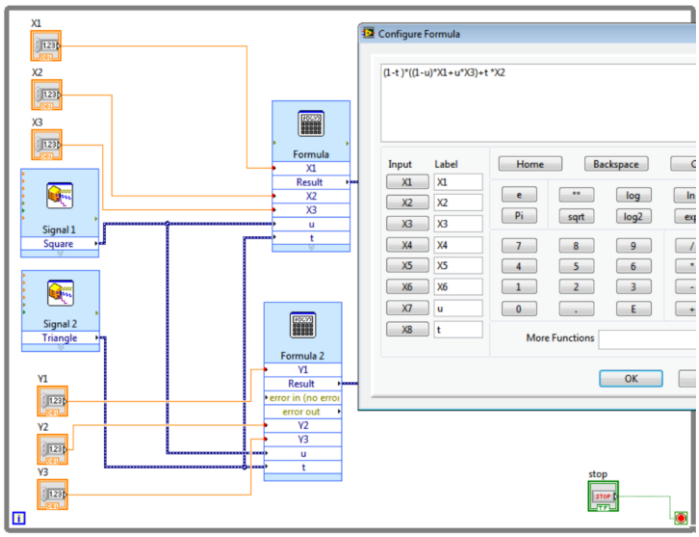

Figure 3.12 Two consecutive straight lines LabVIEW™ program.

The parametric equations of two consecutive straight lines are represented on the system (3.9):

$$\begin{cases}(1-u)\cdot[(1-t)x_1+t\cdot x_2]+u\cdot[t\cdot x_2+(1-t)x_3] \\ (1-u)\cdot[(1-t)y_1+t\cdot y_2]+u\cdot[t\cdot y_2+(1-t)y_3]\end{cases} \quad (3.9)$$

However, to be possible to perform these programs, it is necessary to use two synchronized time variables, **u** and **t**. In this case, **u** is a square signal and **t** is a triangle signal (LabVIEW™ language). Since their range should be between 0 and 1, their offset and amplitude in the program should be set to 0.5.

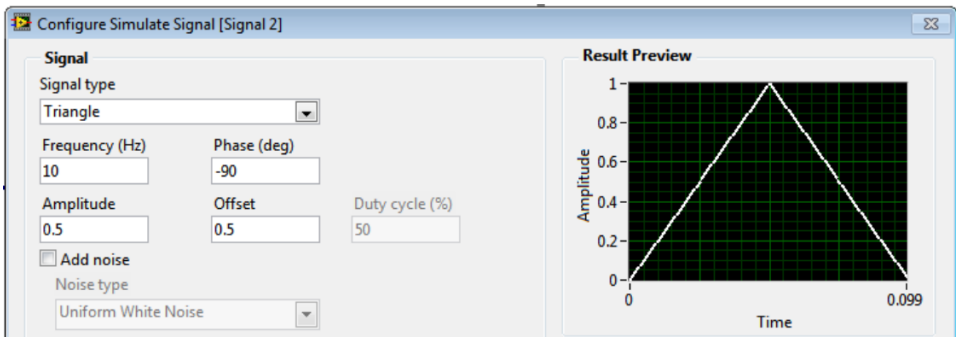

Figure 3.13 Triangle signal configuration

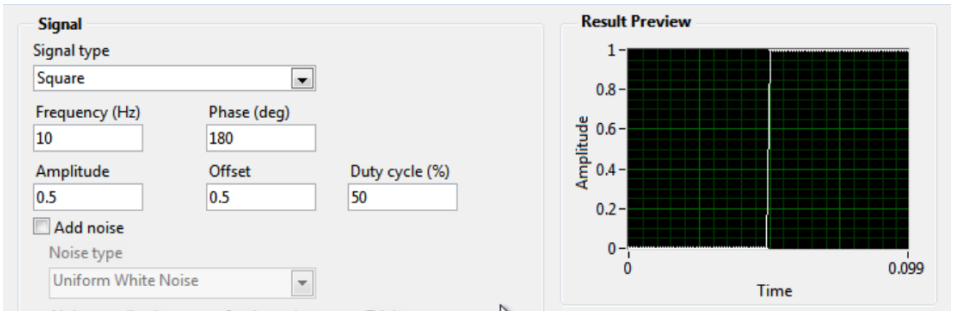

Figure 3.14 Square signal configuration

For instance, the values set on Figures 3.13 and 3.14 can be understood in this way: when u=0, the straight line A-B is performed; when u=1, the straight line B-C is drawn, but with an inversion of time. Both signals have the same period.

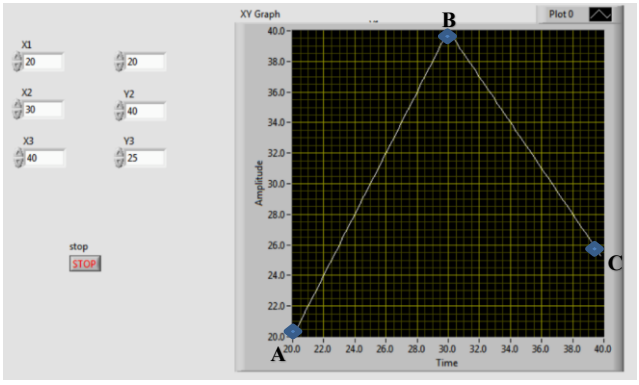

Figure 3.15 Two consecutives straight lines drawn in LabVIEW™.

3.4. Curvilinear trajectories

3.4.1. Bézier's curves

To study the feasibility of curvilinear trajectories with the software in issue, a smooth set of equations was used. More precisely, it was decided to use Bézier's curve equations, of widespread use in computer graphical applications. It has four check points (x_1,y_1), (x_2,y_2), (x_3,y_3) and (x_4,y_4).

Therefore, the systems of equations (3.10) represent a Bézier's curve with four check-points:

$$\begin{cases} x(t) = (1-t)^3 x_1 + 3t(1-t)^2 x_2 + 3t^2(1-t)x_3 + t^3 x_4 \\ y(t) = (1-t)^3 y_1 + 3t(1-t)^2 y_2 + 3t^2(1-t)y_3 + t^3 y_4 \end{cases} \quad (3.10)$$

with $t \in [0; 1]$

However, to improve the system, it was decided to introduce an adaptive law, in regard to the velocity. Accordingly, the time variable, **t**, is replaced by **α**, which is then equal to:

$$t \in [0, t_f] \rightarrow \alpha = \frac{t}{t_f} \therefore \alpha \in [0,1]$$

Therefore the equations respecting to the positions x(t) and y(t) become as follows:

$$\begin{cases} x(t) = \left(1-\frac{t}{t_f}\right)^3 x_1 + 3\frac{t}{t_f}\left(1-\frac{t}{t_f}\right)^2 x_2 + 3\left(\frac{t}{t_f}\right)^2\left(1-\frac{t}{t_f}\right)x_3 + \left(\frac{t}{t_f}\right)^3 x_4 \\ y(t) = \left(1-\frac{t}{t_f}\right)^3 y_1 + 3\frac{t}{t_f}\left(1-\frac{t}{t_f}\right)^2 y_2 + 3\left(\frac{t}{t_f}\right)^2\left(1-\frac{t}{t_f}\right)y_3 + \left(\frac{t}{t_f}\right)^3 y_4 \end{cases} \quad (3.11)$$

Additionally, the system (3.12) show the equations of the velocity (derivating (3.11)):

$$\begin{cases} \dot{x}(t) = -3\left(1-\frac{t}{t_f}\right)^2\left(\frac{1}{t_f}\right)x_1 - 3\frac{t}{t_f^2}\left(1-\frac{t}{t_f}\right)x_2 - 6\frac{t}{t_f^2}\left(1-\frac{t}{t_f}\right)x_2 + 6\frac{t}{t_f^2}\left(1-\frac{t}{t_f}\right)x_3 - 3\frac{t^2}{t_f^3}x_3 + 3\frac{t^2}{t_f^3}x_4 \\ \dot{y}(t) = -3\left(1-\frac{t}{t_f}\right)^2\left(\frac{1}{t_f}\right)y_1 - 3\frac{t}{t_f^2}\left(1-\frac{t}{t_f}\right)y_2 - 6\frac{t}{t_f^2}\left(1-\frac{t}{t_f}\right)y_2 + 6\frac{t}{t_f^2}\left(1-\frac{t}{t_f}\right)y_3 - 3\frac{t^2}{t_f^3}y_3 + 3\frac{t^2}{t_f^3}y_4 \end{cases} \quad (3.12)$$

In order to test the cubic Bézier's equations with adaptive duration (and thus, speed) these equations where inserted in LabVIEW™. Its implementation is shown on Figures 3.16 and 3.17:

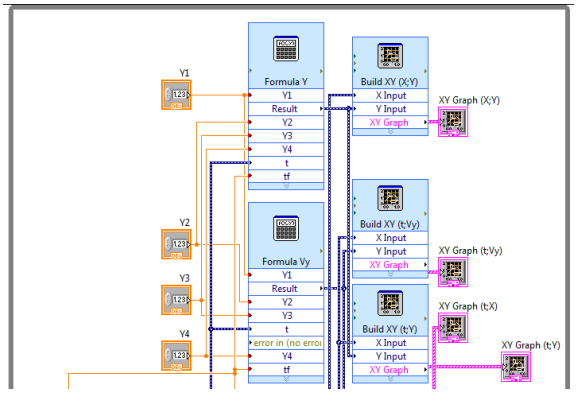

Figure 3.16 Block diagram of cubic Bézier's curve with adaptive velocity on LabVIEW program (1).

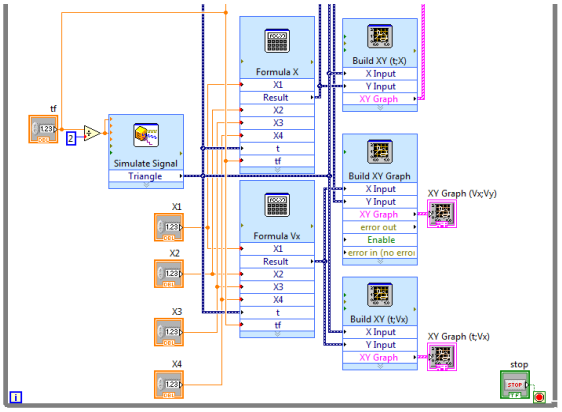

Figure 3.17 Block diagram of cubic Bézier's curve with adaptive velocity on LabVIEW program (2).

And its graphical representation:

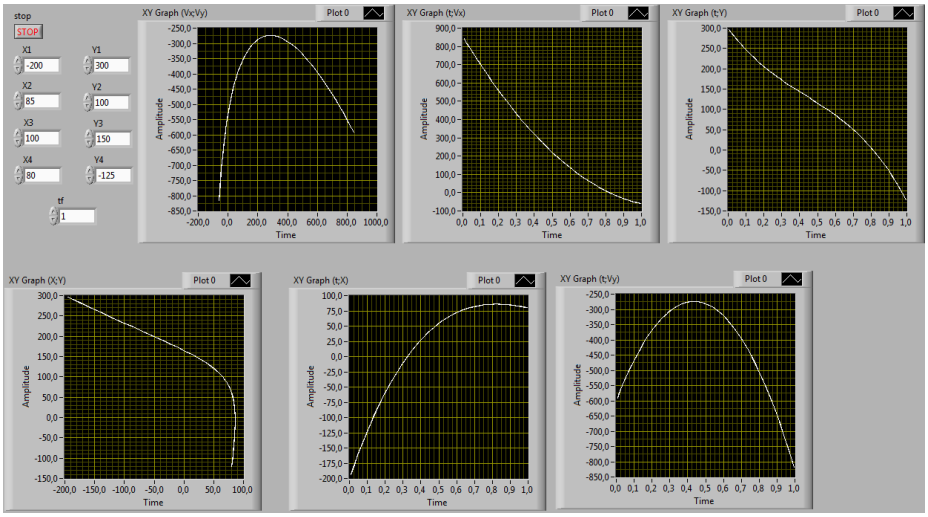

Figure 3.18 Graphical Representation of Cubic Bézier's Curve with adaptive velocity.

The graphs obtained in LabVIEW™ prove the feasibility of curvilinear trajectories on this software. This means that it is actually possible to control the nanometric table along curvilinear trajectories. Once again, by handling the table's voltage the user is

able to deal with the position of the points that he wants. Moreover, the table displacement corresponds to the position graph (x,y) – it is represented on Figure 3.18, left graph of the second row.

3.4.2. **Circle**

In order to test a complete circular trajectory, it was decided to create a LabVIEW™ program with a circle (Figure 3.19).

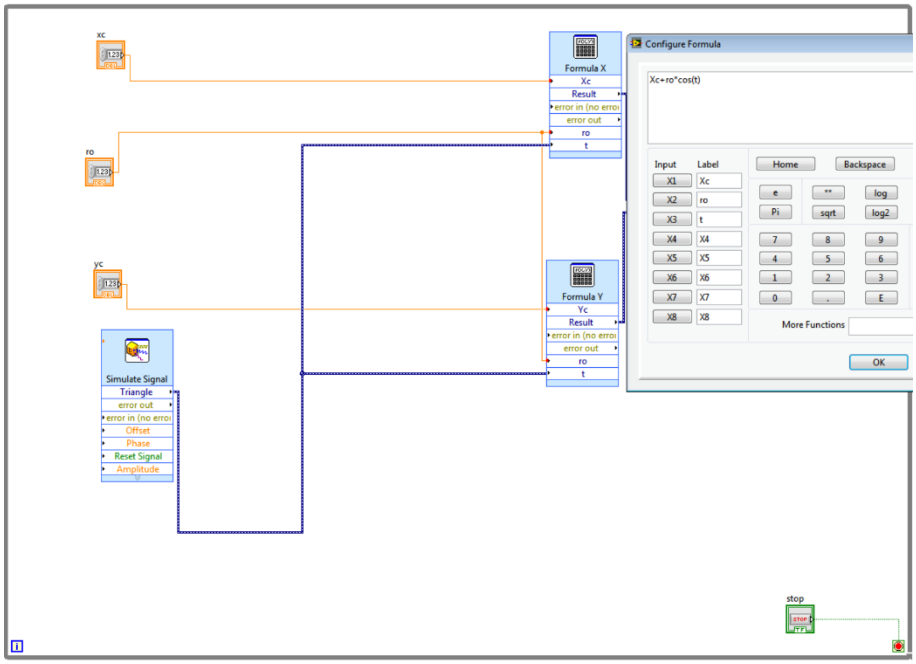

Figure 3.19 LabVIEW's Block Diagram for a circle.

Once again, parametric equations were used. The equations that allows the user to draw a circle is represented in the system (3.13)

$$\begin{cases} x = x_c + \rho \cdot \cos(\theta) \\ y = y_c + \rho \cdot \sin(\theta) \end{cases} \tag{3.13}$$

where $\mathbf{x_c}$ and $\mathbf{y_c}$ are the coordinates of the circle centre and $\boldsymbol{\rho}$ the radius of the circle.

However, the limits of the theta (θ) parameter must be set and this parameter is simulated by a **triangle signal** (Figure 3.20). In this case this parameter's range is from **0** to **2π**.

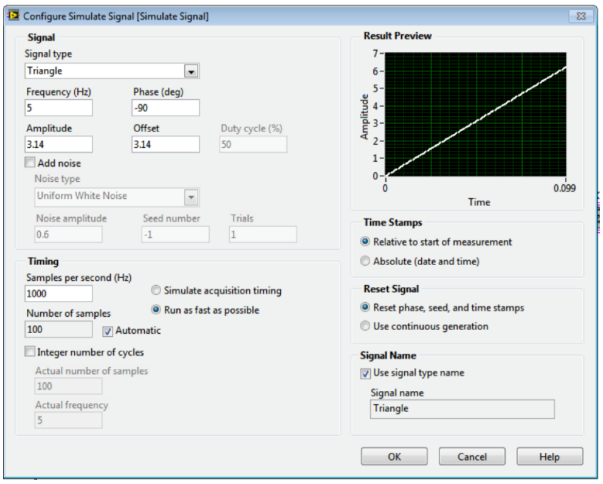

Figure 3.20 Simulate signal setup used.

The amplitude of the signal was set to π, as well as the offset. The frequency is 5 Hz and the phase is -90º. This instructs the program to perform a circle step-by-step (i.e. 0 : step : 2π)

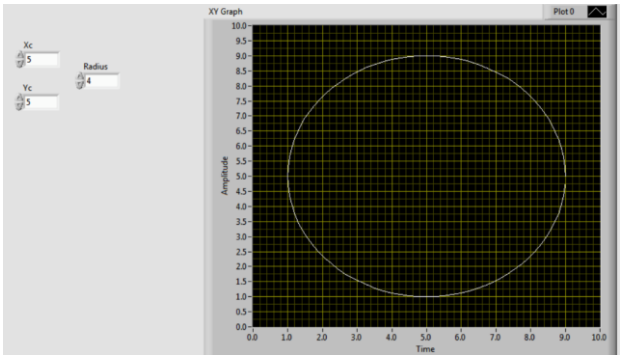

Figure 3.21 Circle drawn using LabVIEW™.

4. MACHINING WITH THE ATOMIC FORCE MICROSCOPE

4.1. Park System's software available

In order to better understand the already mentioned (in section 2) capabilities of the Atomic Force Microscope of Cardiff School of Engineering, and due to the lack of power between the DAQ and the Signal Access Module, some very basic experiences with simple straight grooves were made.

However, to properly machine, there are several parameters that should be carefully set, such as the set point force, the scan size, or the machining mode, using numerous different programs.

Thus, the software that Park Systems (AFM's manufacturer) puts available to its users are:

- XEC **(**Figure 4.1**):** the software that allows the user to launch the camera; in this program the user can see the cantilever and the sample, as well;

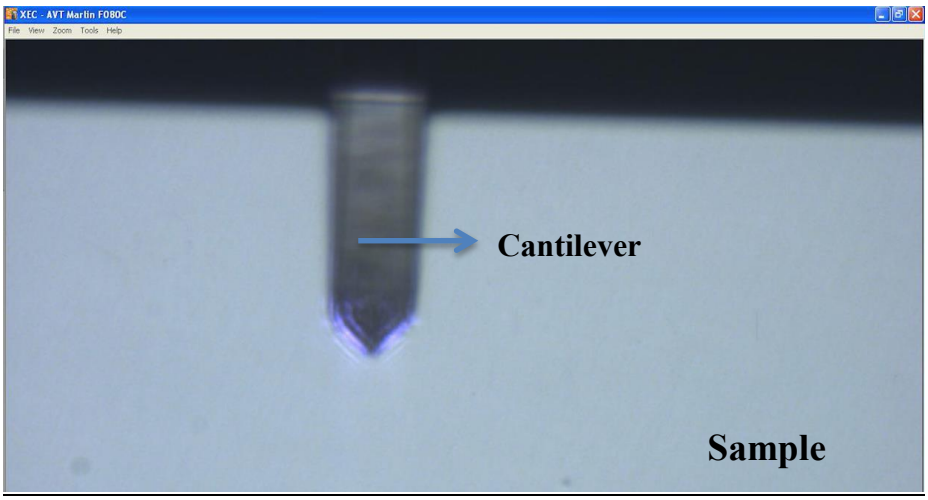

Figure 4.1 XEC software appearance.

- XEL (Figure 4.2): this is the nanolithography tool, where very simple trajectories in the AFM are generated; some important parameters should be set before starting machining, such as:
  - Lithography Mode;
  - MAX and MIN Load (nN);

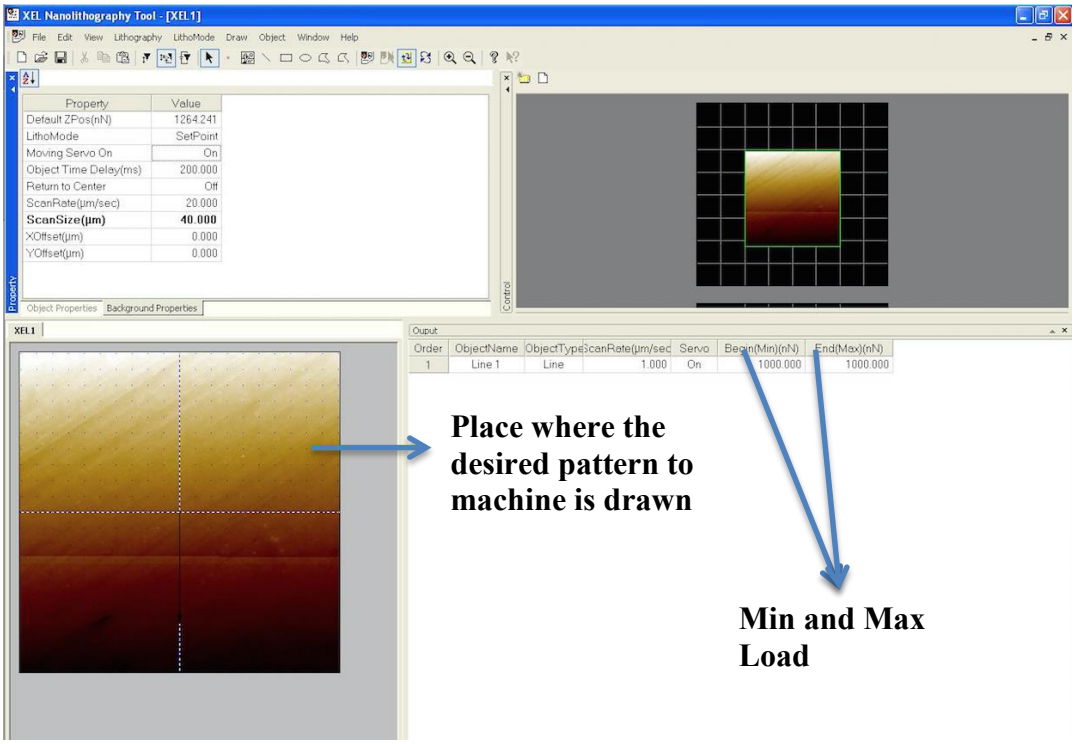

Figure 4.2 XEL software appearance.

- XEI: the program that allows the user to analyse the images obtained after the machining process;
- XEP (Figure 4.3): this is the data acquisition software; here the user needs to set some important parameters, such as the set point force and, when machining, for instance, the scan size; it is also in this program that the operator defines the probe that he is using and the machining mode (contact/non-contact), as well; all the operations related to the displacement of the Z axis and with the microscope's camera are made using this software, too.

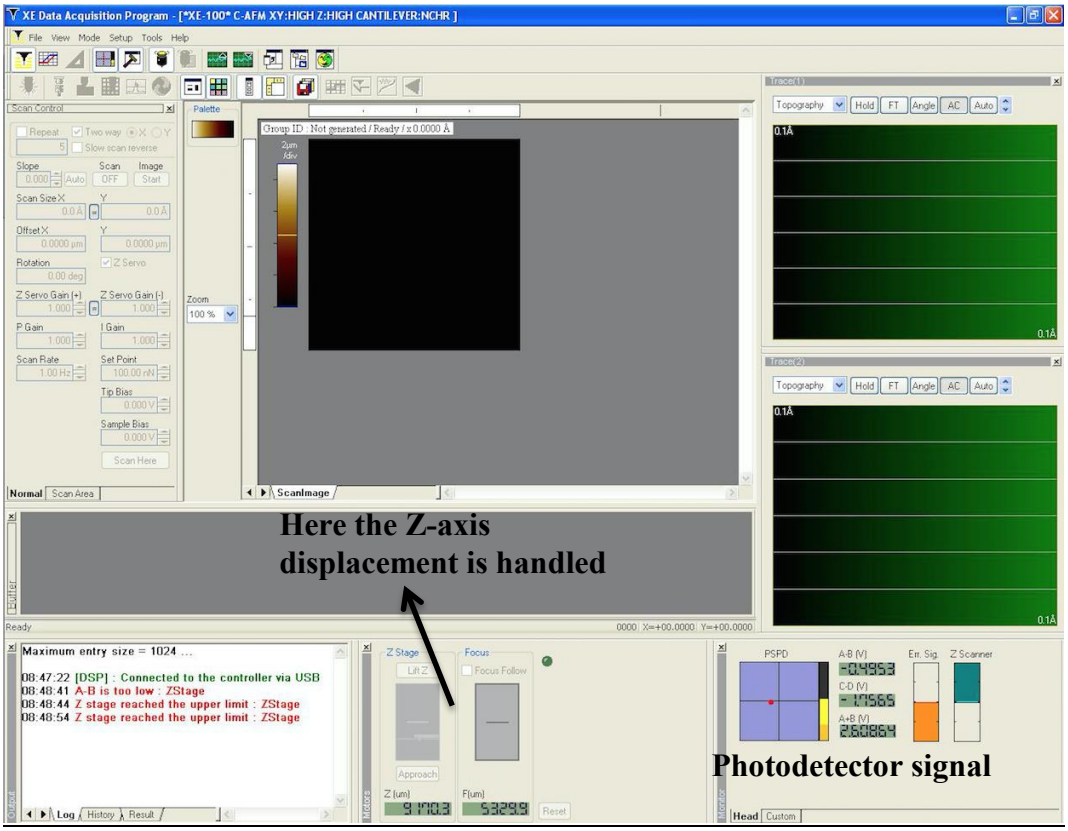

Figure 4.3 XEP software appearance.

4.2. Machining directions

Before proceeding with the explanation of the process of converting the voltage data into cutting force, it might be important to clarify the four possible machining directions, visible in Figure 4.4. All of them are related with the cantilever's default position. This is to say that the direction which the cantilever's edge faces, is considered the forward direction.

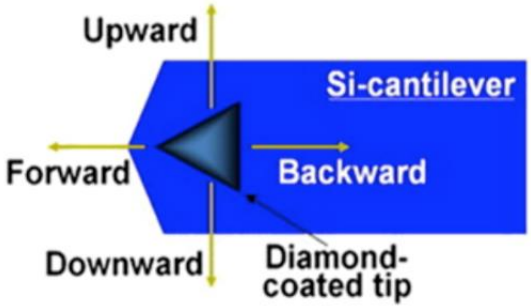

Figure 4.4 Four machining directions (according to the cantilever orientation) [extracted from **(Laot, 2013)**].

4.3. Voltage versus Cutting force

Once the axes of the Atomic Force Microscope are displaced by sending a signal to the piezoelectric actuators of each axes, the response that it is obtained in the PSPD (Position Sensitive Photo Detector) and then in the software that monitors the signal obtained (XEP) comes in voltage. The voltage's feedback when machining is a reflex of the cantilever's deflection (Figure 4.5). An interesting fact, not to be explored in this text is that, as it can be seen in Figure 4.5, depending on the workpiece's movement direction, the deflection (concave, backwardly; convex, forwardly) and the heights of the removed material portion are different.

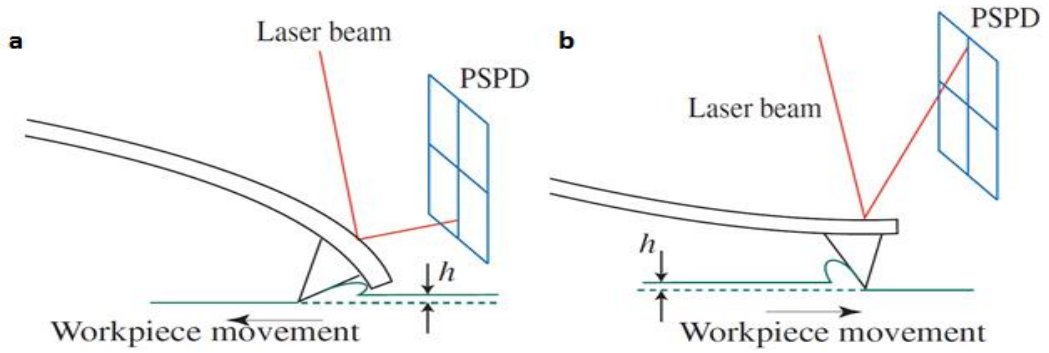

Figure 4.5 Voltage obtained in the PSPD according to the cantilever's deflection [extracted from **(Laot, 2013)**].

Thus, this supra-mentioned voltage can be translated into a cutting force. This latter parameter can be of great importance due to its high relevance for any mechanical machining process, because there are forces that are generated between the cutting tool and the workpiece.

However, the voltage data has no concrete physical meaning. It is just an output from a measuring device. Concretely, in the case of the Atomic Force Microscope, it is fortunately possible to link the voltage output to the deflection of the cantilever, and thus, the force between the tip and the material.

4.4. Cutting force components

There are two components of the force applied when machining: the normal force, and the tangential force (see Figure 4.6). The cutting process has a resultant force, F,

which is usually applied on the tip's edge. The cutting force, F, can be, therefore, decomposed in different orthogonal pairs, depending on the perspective:

- On the workpiece's surface:
  - F_p – penetration force;
  - F_c – cutting force;
- On the edge's tip:
  - F_t – tangential force;
  - F_n – normal force;
- In relation to the cutting plan:
  - F_τ – tangential force;
  - F_σ – normal force;

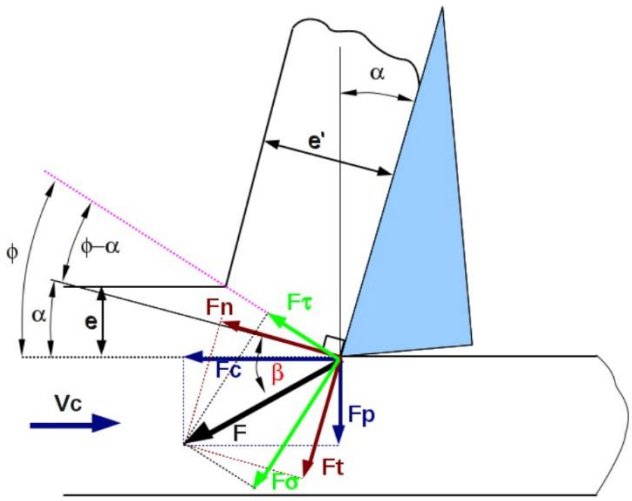

Figure 4.6 Existing force components during the machining process [extracted from **(Simões, 2011/2012)**].

However, as previously mentioned, for the present study, the only forces that will be considered in this study are the normal force, F_n, and the tangential force, F_t; the other forces represented in Figure 4.6 will not be taken into consideration.

To understand how these forces act on the process of machining let's take a look at Figure 4.7.

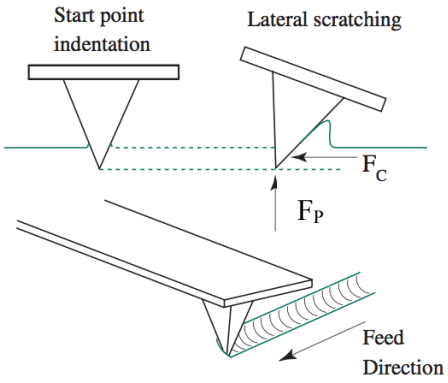

Figure 4.7 Normal and Tangential forces in an AFM machining process [extracted from **(Malekian, Park, Strathearn, Mostofa, & Jun, 2010)**].

Due to the fact that in the article where the image was extracted from the authors are using different terms and notation for what the author of this thesis call normal and tangential forces, please take in consideration that:

$\Rightarrow$ F_P (Penetration Force) – (Malekian, Park, Strathearn, Mostofa, & Jun, 2010) = TANGENTIAL FORCE

$\Rightarrow$ F_C (Cutting Force) – (Malekian, Park, Strathearn, Mostofa, & Jun, 2010) = NORMAL FORCE

4.5. Voltage into Cutting Force translation

In order to collect the voltage data gathered by the Signal Access Module after the machining task, a program in LabVIEW™ was used (depicted on Figure 4.8). It collects four different data (also because the DAQ Module 9223 has four channels): apart from the A-B voltage, it gathers the voltage variation concerning the Y and Z-axes displacement, and the Lateral Force Measurement, as well.

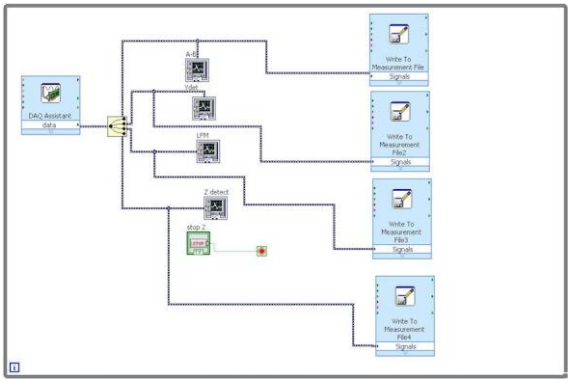

Figure 4.8 LabVIEW™ data gathering interface.

There are several methods to compute the two forces that matter for the present report. Two different methods will be used, one for each force (normal and tangential). They are described in several papers, such as (Varenberg, Etsion, & Helpering, 2003) and (Cannara, Eglin, & Carpick, 2006).

4.5.1. The normal force

This force is always present when machining, and it is perpendicular to the cantilever. It is the force that the surface imposes on the cantilever as an opposition to the effort of the cantilever on the surface, when machining (Newton's 3rd Law – Action/Reaction).

The expression (4.1) can be simply understood if one relate it with the differential equation of the elastic line (where the bending's displacement is directly proportional to the applied load). In this case, specifically, the cantilever's bending will be proportional to the force applied on its tip. Thus, the expression that allows to compute the normal force is represented by the equation (4.1):

$$F_n = ß \cdot V_{A-B} \tag{4.1}$$

being $V_{A\text{-}B}$ the voltage on the PSPD, which is divided in four quadrants, as depicted on Figure 4.9.

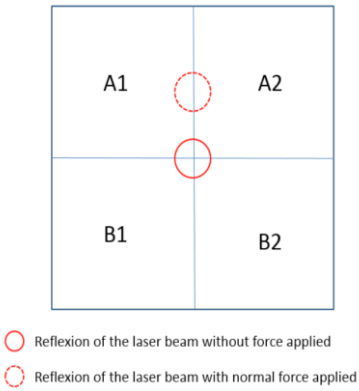

Figure 4.9 Voltage A-B on the Photodiode [extracted from **(Laot, 2013)**].

The fact that the feedback obtained in the PSPD during a machining process is directly related with the cantilever's deflection (in this case), should be highlighted.

This voltage is a result of $V_{A-B} = (V_{A1} + V_{A2}) - (V_{B1} + V_{B2})$. The coefficient ß is the normal calibration constant. Quoting (Cannara, Eglin, & Carpick, 2006), the expression that permits us to calculate it, is shown on the expression (4.2):

$$ß = \frac{K_N S_N}{\cos \varphi} \tag{4.2}$$

with:

- K_N: The normal spring constant; this value is always given by the manufacturer;
- S_N: The normal sensitivity; usually, the calibration straight line graph comes in the manufacturer's information leaflet, as well;
- φ: The angle of the cantilever, in relation to the machining surface;

4.5.2. The tangential force

Like the normal force, this force is also always present. However, when we are dealing with nano-indendation processes this force does not exist (i.e. when there is no lateral movement).

Similarly to the normal force, the tangential force is also related to the voltage displayed on the photodiode, but the relationship between the quadrants is different. Equation (4.3) represents the tangential force:

$$F_t = \alpha \cdot V_{C-D} \tag{4.3}$$

being $\mathbf{V_{C\text{-}D}}$ the voltage on the PSPD, but in this case, the reflection of the laser beam is slightly different from the normal force, as it is depicted on Figure 4.10.

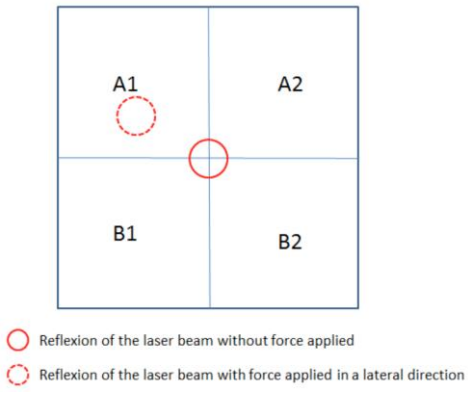

Figure 4.10 Voltage C-D (after applying the conversion) on the Photodiode [extracted from **(Laot, 2013)**].

Therefore, the voltage C-D can be obtained doing $V_{C-D} = (V_{A1} + V_{B1}) - (V_{A2} + V_{B2})$. The parameter α is the tangential calibration constant.

In order to compute the parameter α another method must be used. It is named "Wedge method", developed by (Ogletree, Carpick, & Salmeron, 1996) and then protracted

by (Varenberg, Etsion, & Helpering, 2003) and (Cannara, Eglin, & Carpick, 2006), and also explained in the thesis report of a previous ENSAM student, David Laot – (Laot, 2013) .

4.5.2.1. The Wedge Method

Due to the fact that, for the tangential force calculation, the spring constant is unknown, there is the need of using the wedge method, which is slightly more difficult than the approach used to compute the normal force. In this technique, a specific sample, with "ups" and "downs" (similarly to steps), was used. It has both flat and sloped surfaces, which make a certain angle between them, as it is depicted on Figure 4.11.

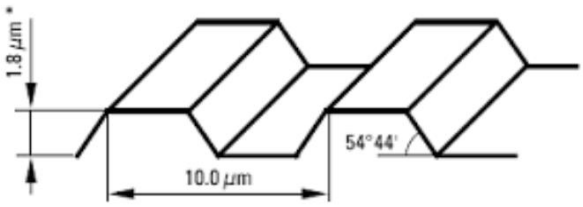

Figure 4.11 Calibration sample used for the wedge method [extracted from **(Laot, 2013)**].

This sample is used in order to measure the C-D voltage along both surfaces (flat and surface) in two different directions (upward and downward) – as it is visible on Figure 4.12. Therefore, after obtaining a difference on the signal according to the sample's slope and after using several formulas concerning these variations, the α parameter can be finally determined:

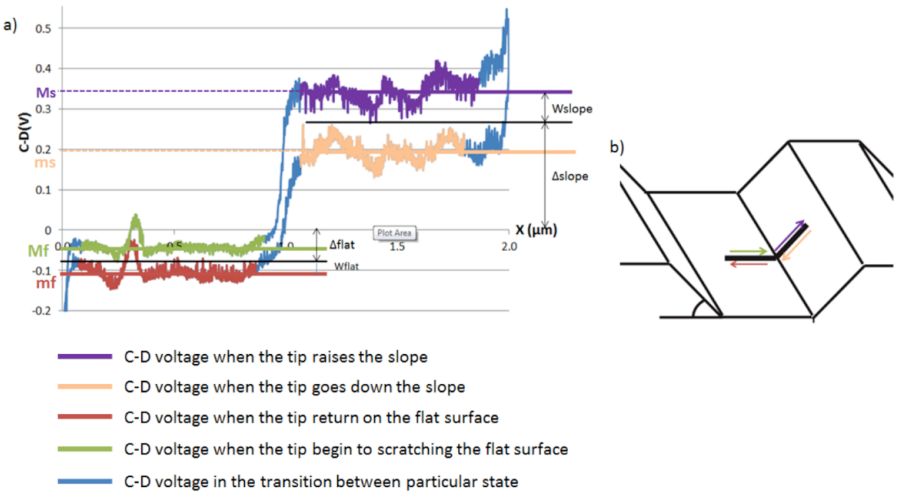

Figure 4.12 a) Signal C-D obtained after using the sample; b) Scheme of the signal measurement procedure (upward and downward direction) [extracted from **(Laot, 2013)**].

The image above, extracted from David Laot's report, was here placed, once it is really clear (a similar image is shown later on Figure 5.10). It helps us to compute the quantities shown in expressions (4.4), (4.5), (4.6) and (4.7), concerning the C-D signal variation, according to the sample's flat and sloped surface.

$$W_{slope} = \frac{M_s - m_s}{2} \quad (4.4) \qquad \Delta_{slope} = \frac{M_s + m_s}{2} \quad (4.5)$$

$$W_{flat} = \frac{M_f - m_f}{2} \quad (4.6) \qquad \Delta_{flat} = \frac{M_f + m_f}{2} \quad (4.7)$$

After obtaining all these values, the formulas that (Varenberg, Etsion, & Helpering, 2003) developed can be directly applied. They are represented on equations (4.8) and (4.9). However, the desired coefficient, $\boldsymbol{\alpha}$, cannot be yet obtained. What it is possible to extract from the following expression is the friction coefficient, $\mu_{\mathbf{w}}$:

$$sin\theta(Lcos\theta + A)\mu_w^2 - \frac{\Delta_{slope} - \Delta_{flat}}{W_{slope}}(Lcos\theta + A)\mu_w + Lcos\theta\ sin\theta = 0 \quad (4.8)$$

with:

- θ: the slope's angle, given by the sample's manufacturer;
- L: the set point force, in nN, that the user pre-defines before the machining process begins;
- A: the adhesion force, given by the XEI software;

Since the previous equation is a quadratic one, two values of $\mu_{\mathbf{w}}$ are obtained. Since one of them is negative, the remaining one is picked, in order to finally compute the $\boldsymbol{\alpha}$ coefficient:

$$\alpha W_{slope} = \frac{(Lcos\theta + A)\mu_w}{cos^2\theta - \mu_w^2 sin^2\theta} \quad (4.9)$$

Lastly, the $\boldsymbol{\alpha}$ coefficient needs to be replaced, in the tangential force expression (4.3).

5. CARDIFF'S AFM EXPERIMENTS

5.1. Methodology

After having well understood the working principle of Cardiff's AFM and all the software necessary to make and analyse a groove, as well as the methods to perform the translation from voltage to cutting force, three different experiments were made. These tests were considered sufficient to understand the differences between applying a lower or a higher load, or even machining in different directions. The parameters considered relevant, in order to evaluate the grooves performed and the pile-ups formations, as well, are their **width** and **height.**

Further, after obtaining all the variables needed to translate voltage into cutting force, new grooves were performed and their data were gathered, in order to obtain the A-B and C-D signals that will allow to get the desired parameters.

5.1.1. Machining process – Z displacement (cantilever behaviour)

To evaluate the probe's behaviour when the user orders the AFM software to begin the machining process, the voltage data gathered with LabVIEW™ was plotted, and the following graph was obtained:

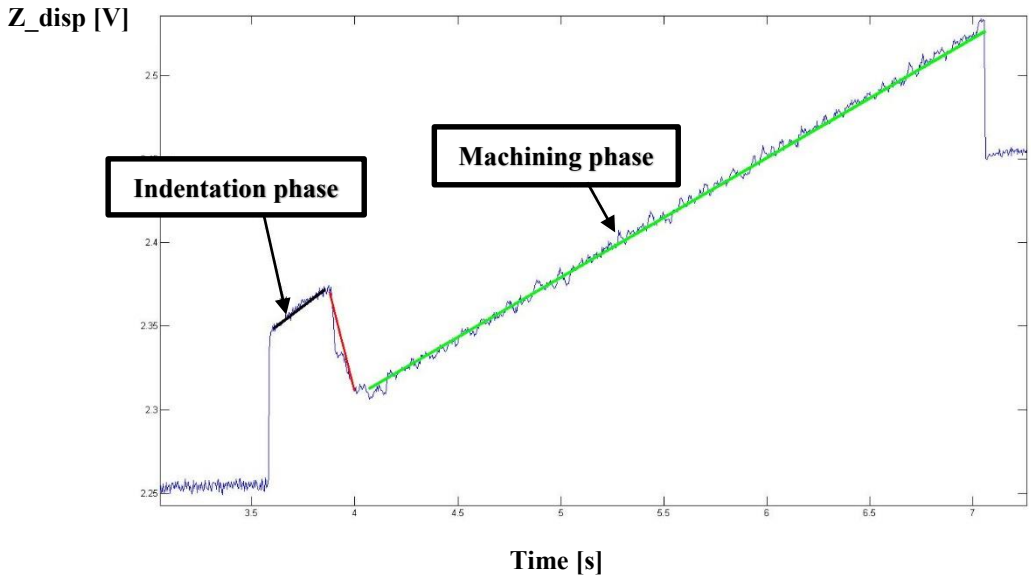

Figure 5.1 Z-axis voltage variation during a groove machining.

Before analysing the image it is important to refer that whenever there is an increase in voltage, in respect to the Z-axis, it means that the cantilever is approaching the sample, and conversibly, when the voltage decreases the tip is going up.

Therefore, as shown in Figure 5.1, initially, the tip approaches the sample (the voltage increases) and then it encounters the sample and the indentation process occurs – black zone. Then, the Z-axis goes up a little bit, and this might happen due to the normal force acting on the cantilever, what makes it to retract – red zone. Finally, the machining process starts, and the groove is made – green zone. The reason why there is a slight slope on the green straight line, instead of a flat straight line, is that the sample is not flat. Hence, three different phases can be distinguished: indentation (black line); scratching (green line); lifting up on the cantilever (after the green line).

5.2. Load comparison

To establish the differences in terms of voltage (and thus, cutting force) two very simple straight grooves were made, one with a high load and one with a low load, in the same direction (forward).

When performing experiments like this, and to obtain the best possible machining profile, the setup probe-sample should be carefully chosen. In this case, since our main objective was to perform visible grooves, a probe with a high stiffness was chosen and a not so stiff simple was picked.

Thus, the cantilever used was a DNISP EB2 one. The sample used to scratch was Single Crystal Copper.

The setup used in Cardiff's Atomic Force Microscope is presented on Table 5-1:

Table 5-1 Machining parameters for grooves 1 and 2.

Groove	Direction	Set point [nN]	Max load [nN]	Velocity [µm/sec]
1	Forward	1000	20000	5
2	Forward	1000	10000	5

5.2.1. Set point vs. Max load

Before presenting the results obtained it is important to make a distinction between the terms set point and max load. In a machining process the set point force can be

considered the first contact force (in this case, it means that the tip did not go inside the sample, yet). In order to avoid damaging the probe's tip, this force should be carefully set up before starting the machining task and it should not be a very high value. Then, the max load force can be understood as the effort that the cantilever applies during the whole machining force, in order to be able to remove the material.

5.2.1.1. **Result analysis**

After having machined the two grooves with different loads, the sample was scanned in order to obtain the profile of the two grooves. In this case, the AFM setup was changed. Here, a cantilever for scanning purposes (ISC 300) was used. Obviously, this type of scanning tasks needs to be performed in **non-contact** mode.

A scanning size of 10.0 µm was used, along the X-axis, which means that the microscope is constantly making displacements of 10.0 µm, from +X to –X.

Once again, LabVIEW™ software was used to gather the data from the scanning task. The files generated were plotted, in order to obtain the groove profile. The corresponding images are depicted here (Figure 5.2a and b and Figure 5.4a and b). Moreover, the graphs have some points tagged on them that will be useful to find the groove height and width (in relation to pileups – points **1** and **2** – and in relation to the groove itself – points **1.1** and **1.2**).

- **GROOVE 1:**

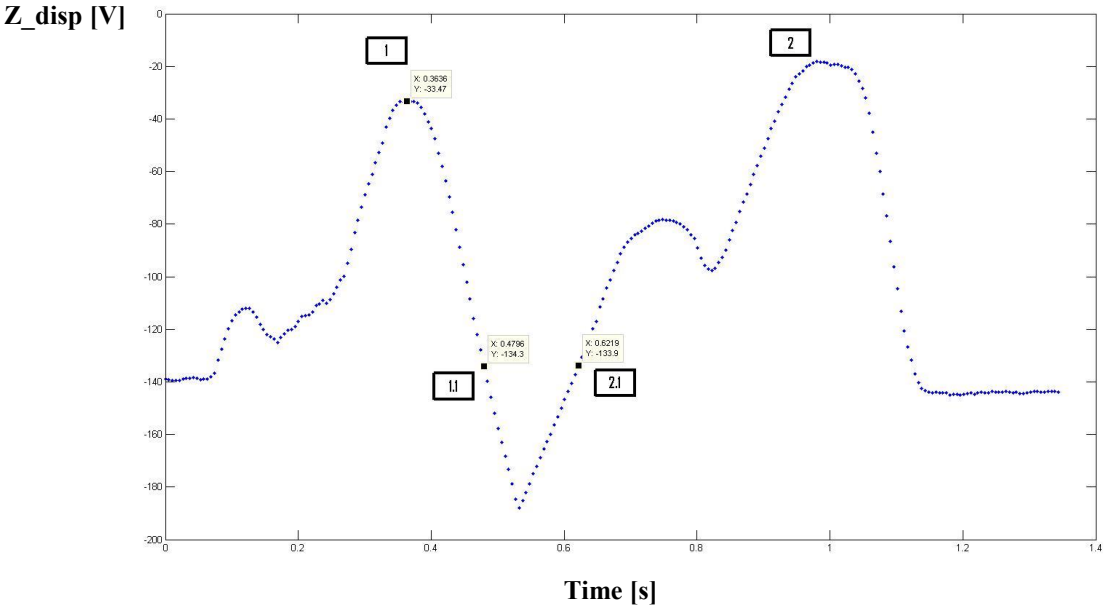

Figure 5.2a Groove 1 profile (the labelled points correspond to the WIDTHS).

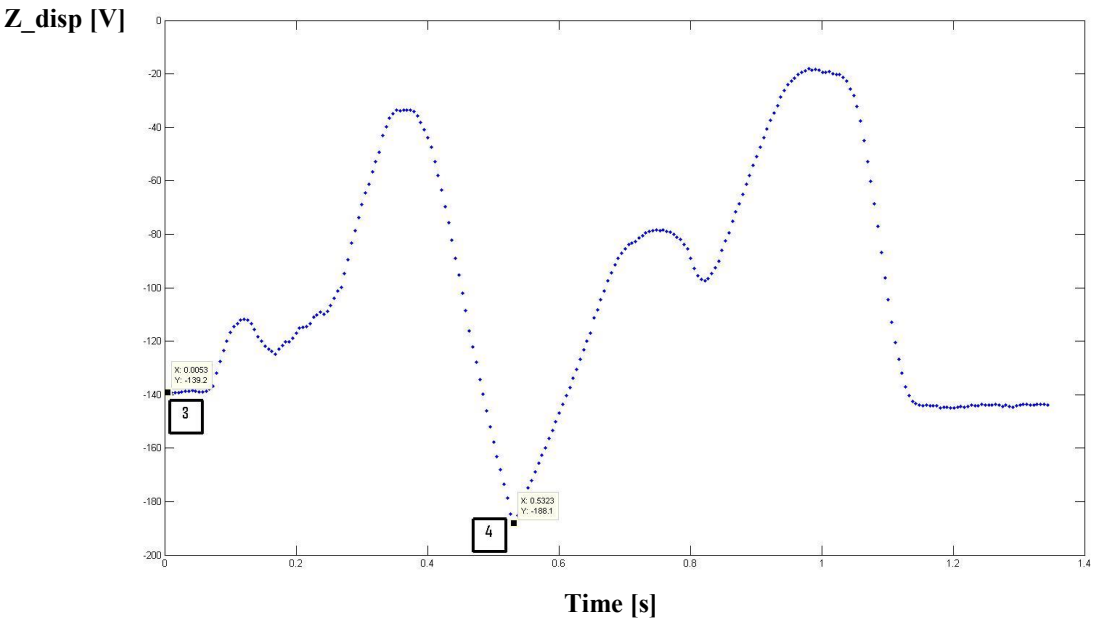

Figure 5.2b Groove 1 profile (the labelled points correspond to the HEIGHT).

In order to have a better notion of the groove, some 3D images of the grooves' topography were created, which can be compared to the 2D graphs. However, due to a limitation of time, it was not possible to obtain all the topographies. Some of those will be shown in this report. Hence, for groove 1, here is its topography, depicted on Figure 5.3:

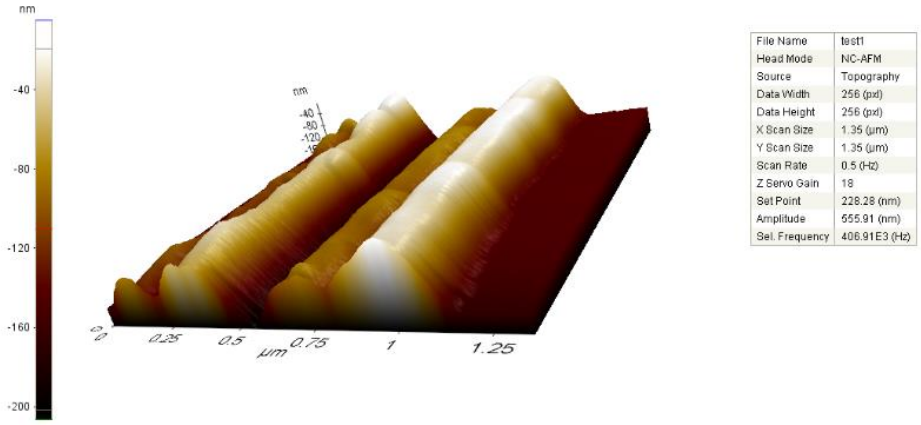

Figure 5.3 Groove 1 topography obtained with XEI.

- **GROOVE 2:**

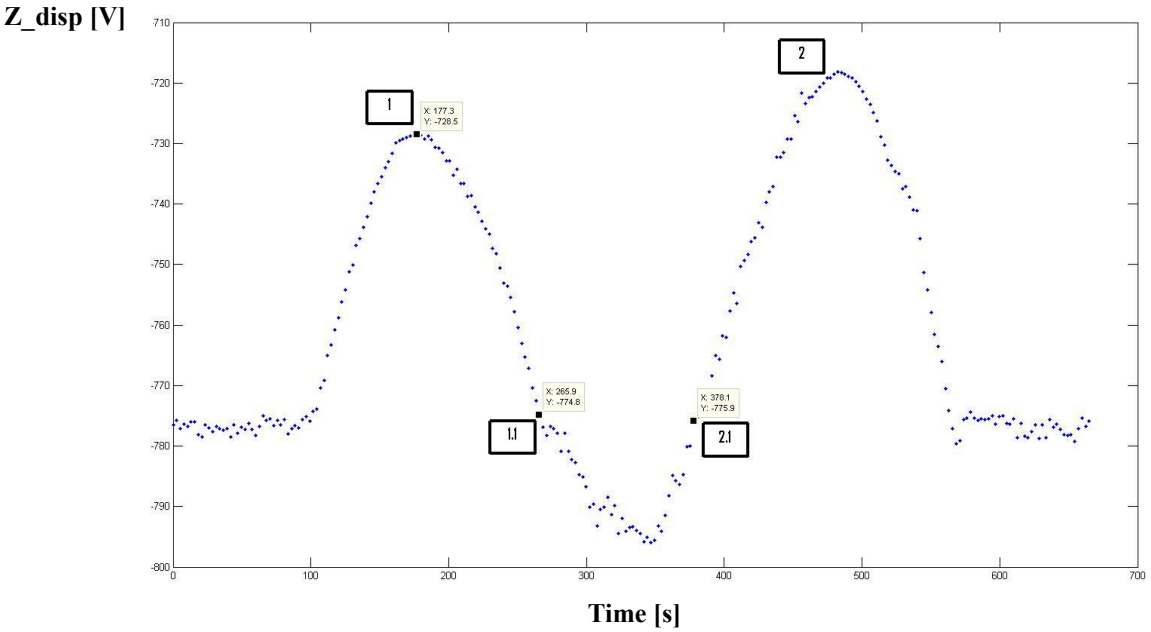

Figure 5.4a Groove 2 profile (the labelled points correspond to the WIDTHS).

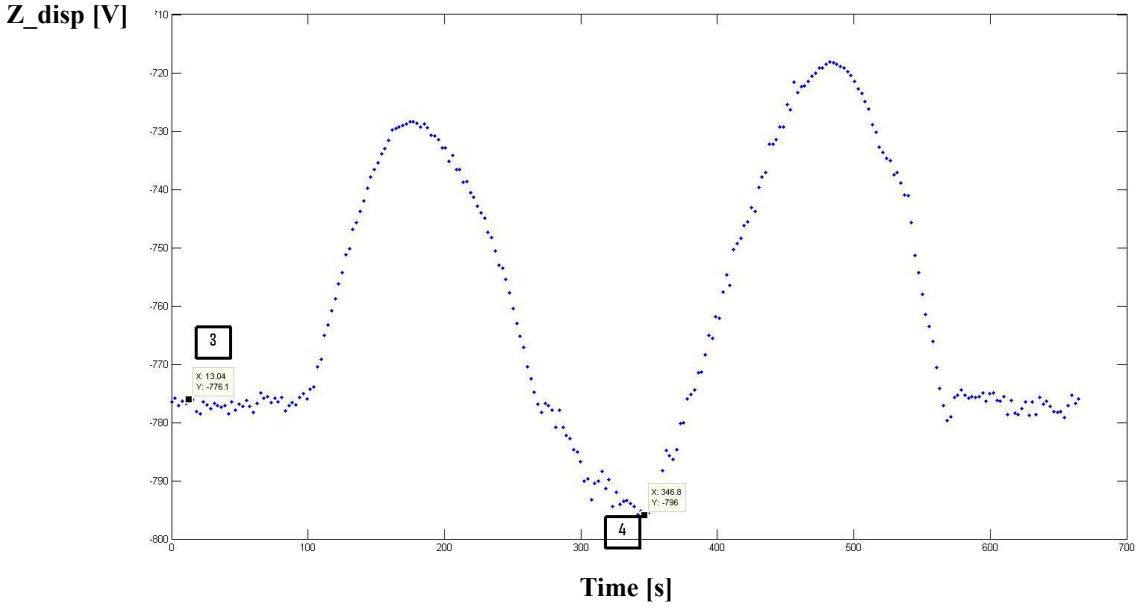

Figure 5.4b Groove 2 profile (the labelled points correspond to the HEIGHT).

In order to find the widths and height of the attained grooves, some points need to be considered. Their measures are presented in Table 5-2:

Table 5-2 Coordinates from the points extracted from the grooves' profile.

Groove	Points	X (nm)	Y (nm)	ΔX (nm)	ΔY (nm) – absolute value
1	1	363.6	-33.47	**632.4**	14.81
	2	996.0	-18.66		
	1.1	479.6	-134,3	**142.3**	0.4
	2.1	621.9	-133.9		
	3	5.3	-139.2	527.0	**48.9**
	4	532.3	-188.1		
2	1	177.3	-728.5	**305.0**	10.3
	2	482.3	-718.2		
	1.1	265.9	-774.8	**112.2**	1.1
	2.1	378.1	-775.9		
	3	13.04	-776.1	333.76	**19.9**
	4	346.6	-796.0		

The highlighted points (in yellow) are of interest to us, in order to evaluate the widths and the height. For the groove's width, the differences between the X coordinates, and for the groove's height, the difference between the Y coordinates, are considered. The X coordinates from groove 2 were converted from μm to nm. They are represented on Table 5-3:

Table 5-3 WIDTHS and HEIGHT of grooves 1 and 2.

GROOVE	WIDTHS (nm)		HEIGHT (nm)
	Between Pile-Ups	Groove	
1	632.4	142.3	48.9
2	305.0	112.2	19.9

5.2.1.2. Conclusion

As expected, the groove made with a load of 10000 nN is shallower than the other one (19.9 < 48.9), since the higher our load is the deeper groove obtanied. The same

happens with the width between pile-ups, since groove 1 is larger than groove 2 (632.4 > 305.0).

As it is shown in both Figure 5.2, the grooves are not perfect. Inside them, there was some material that was accumulated on the right side of the groove. This may occur due to the shape of the tip, since one of its faces was pushing the material in one direction, and then, the other face pushed the material further (namely to the right side).

However, if the table above is considered, in which concerns the width between the walls of the scratched surface (groove), it is easy noticeable that, though the value for groove 1 is higher than for groove 2 (142.3 vs. 112.2) its ratio is much lower than the ratio between the width between pile-ups (142.3/112.2 vs. 632.4/305.0). This is due to the formation of that secondary pile-up explained above.

Furthermore, if the pile-ups formation is compared it can be concluded that if a higher load is applied, the accumulation of pile ups will be much higher than if a machining process with a lower load is made. For this reason, the profile of groove 2 is much smoother than the profile of groove 1 (Fig. 51 vs. Fig. 49). This is quite obvious because when higher loads are applied, the tip goes deeper, which means that more material will be removed and more pile-ups will arise.

5.3. Direction comparison

Another aspect that may influence a pattern is the machining direction. To verify whether the direction affects or not the groove profile, two different grooves were made with the same lade but in the opposite direction.

Table 5-4 shows the setup used in the tests performed:

Table 5-4 Machining parameters for grooves 1 and 3.

Groove	Direction	Set Point [nN]	Max Load [nN]	Velocity [µm/sec]
1	Forward	1000	20000	5
3	Backward	1000	20000	5

Basically, groove 1 is the same used for the test before. Groove 3, as mentioned before, was done in backwards direction, with the same load as groove 1.

5.3.1.1. **Result analysis**

The cantilever used to perform the grooves' scanning was the same used for the load comparison test, as well as the scanning size according with the X-axis. LabVIEW was used to gather all the data extracted from the test.

As done for the previous analysis, the profile of groove 3 is depicted on Figure 5.5a and b. Groove 1 profile is already depicted on Figure 5.2a and b.

- **GROOVE 3:**

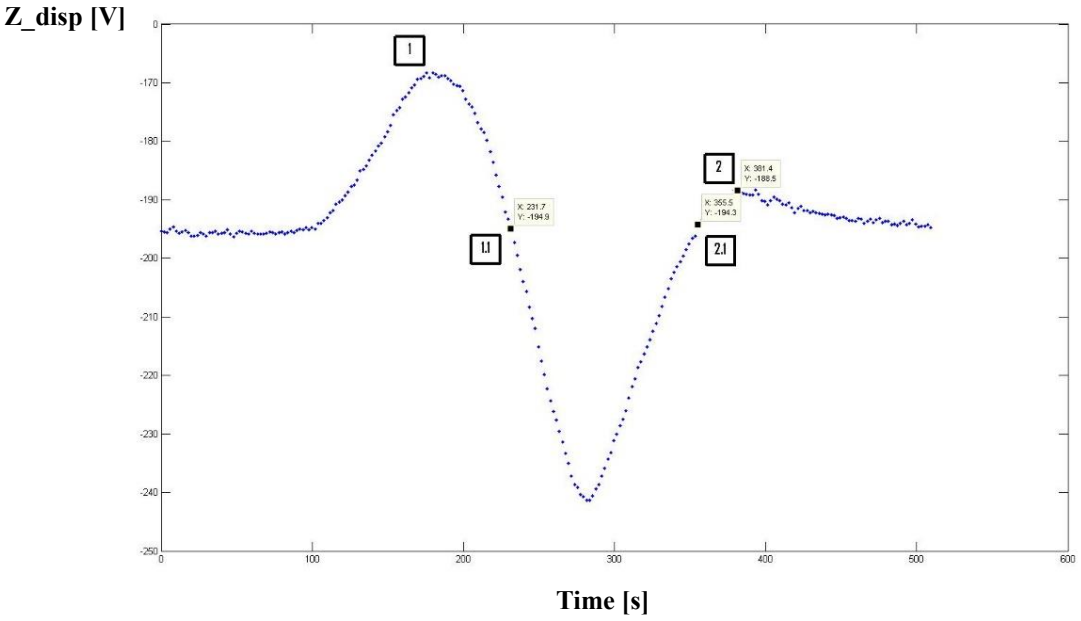

Figure 5.5a Groove 3 profile (the labelled points correspond to the WIDTHS).

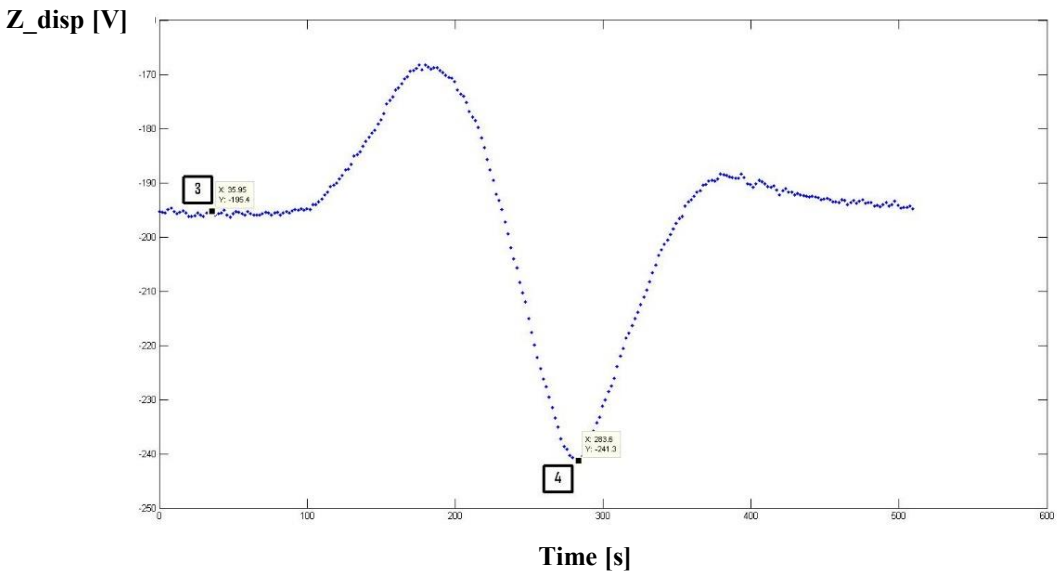

Figure 5.5b Groove 3 profile (the labelled points correspond to the HEIGHT).

The points' coordinates of groove 3 profile necessary to measure the widths and the height are shown on Table 5-5:

Table 5-5 Coordinates from the points extracted from the grooves' profile.

Groove	Points	X (nm)	Y (nm)	ΔX (nm)	ΔY (nm) – absolute value
3	1	181.7	-168.6	199.7	19.9
	2	381.4	-188.5		
	1.1	231.7	-194.9	123.8	0.6
	1.2	355.5	-194.3		
	3	35.95	-195.4	247.65	45.9
	4	283.6	-241.3		

Therefore, the width and height of each groove is shown on Table 5-6:

Table 5-6 WIDTHS and HEIGHT of grooves 1 and 3.

GROOVE	WIDTHS (nm)		HEIGHT (nm)
	Between Pile-Ups	Groove	
1	632.4	142.3	48.9
3	199.7	123.8	45.9

In the case of groove 3, XEI was used to obtain the profile of the groove and its 3D topography, as well (Figure 5.7). They look like this:

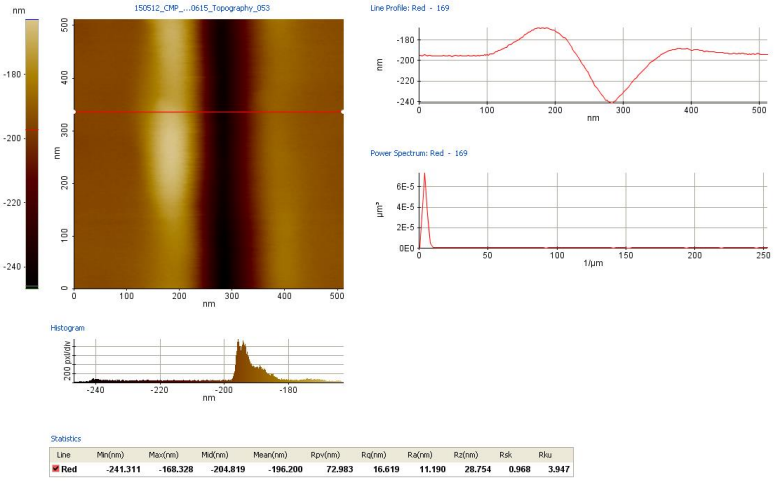

Figure 5.6 Groove 3 profile obtained with XEI.

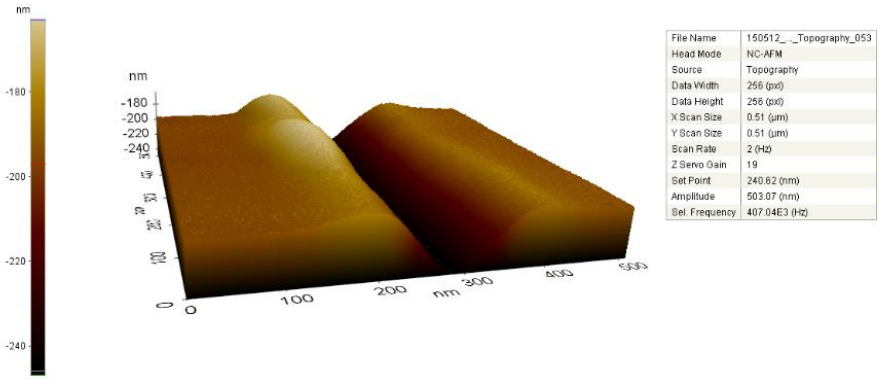

Figure 5.7 Groove 3 topography obtained with XEI.

5.3.1.2. **Conclusions**

In order to get more concrete conclusion, in this section all the grooves will be compared. Therefore, despite groove 3 having a much smoother appearance, it seems that performing machining in another direction has a high influence on the resulting groove, at least in which respects to the width, since groove number 3 is narrower than groove 1 and also than groove 2. Moreover, though machining in a different direction than groove 2, groove 3 is much deeper, which is not strange due to the load applied (10000 nN against 20000 nN). Finally, if grooves 1 and 3 are compared in terms of height, they have a slight difference (3 nm), which means that the machining direction does not affect the groove's depth when the same load is applied.

5.4. Voltage into Cutting Force conversion

After describing the process that must be followed to convert the voltage data into cutting force, let's explain how the method was applied using Cardiff's AFM.

Basically, there are two parameters, α and β, which needs to found, in order to compute F_N and F_T.

The first one can be directly calculated using equation (4.2), once the characteristics of the cantilever (DNISP EB2) are known, which are provided by its manufacturer.

Furthermore, to determine the normal sensitivity, S_N, and the spring constant, K_N, it is necessary to perform a force-displacement (FD) test, which consists in putting the cantilever in contact with a hard surface. It is a kind of a hardness test. Fortunately, this test was contemplated in the manufacturers' data paper. All the values of the FD test were extracted to Table 5-7.

Table 5-7 Force-Displacement test data.

Deflection (V)	Deflection (m)	Force1 (mg)	Force2 (mg)	Force1 (N)	Force2 (N)
-5.0	-1.37E-06	6.7	6	6.571E-05	5.884E-05
-4.0	-1.10E-06	13.7	12.8	1.344E-04	1.255E-04
-3.0	-8.22E-07	19.8	18.7	1.942E-04	1.834E-04
-2.0	-5.48E-07	25.0	24.1	2.452E-04	2.363E-04
-1.0	-2.74E-07	31.2	30.2	3.060E-04	2.962E-04
0.0	0.00E+00	36.7	35.9	3.599E-04	3.521E-04
1.0	2.74E-07	43.2	41.2	4.237E-04	4.040E-04
2.0	5.48E-07	49.6	47.8	4.864E-04	4.688E-04
3.0	8.22E-07	57.4	53.9	5.629E-04	5.286E-04
4.0	1.10E-06	63.8	60.2	6.257E-04	5.904E-04
5.0	1.37E-06	72.3	67.3	7.090E-04	6.600E-04

With this data, the graph corresponding to the relation between the force applied and the cantilevers deflection, which will give us the spring constant, can be plotted (Figure 5.8).

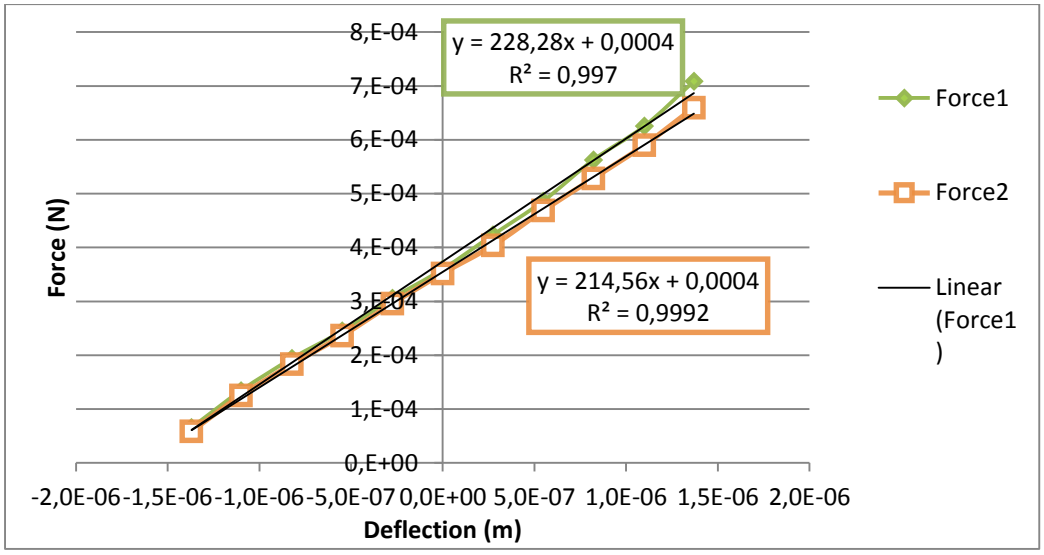

Figure 5.8 Force/Deflection graph (to obtain the Spring Constant).

Since two different values were obtained, the average was computed to get an approximate value of 221 N/m. This means that K_N=**221 N/m**.

According to the finding of a PhD student, who performed a similar test in Cardiff, the other value, S_N, is equal to **0.0165 µm/V**. Moreover, the angle of the cantilever with respect to the sample surface, φ, is approximately **12º**.

Then, replacing the corresponding values on equation (4.2):

$$\text{ß}=3.73\ \mu N/V$$

Furthermore, in order to find the second calibration parameter, α, the calibration sample used for this method was scanned. The setup used for the scanning process is presented on Table 5-8:

Table 5-8 AFM setup used to scan the calibration sample.

Sample	MicroMasch TGF11
Cantilever	DNISP EB2 (same that was used for machining)
Machining Mode	Contact Mode
Process	Scanning (2x256)
Scan Rate [Hz]	0.5
Scan Size X [µm]	10.0
Set Point [µN]	1.2

As explained before, and as shown on Figure 5.9 (scanning image obtained with XEC) this sample is made of several bumps.

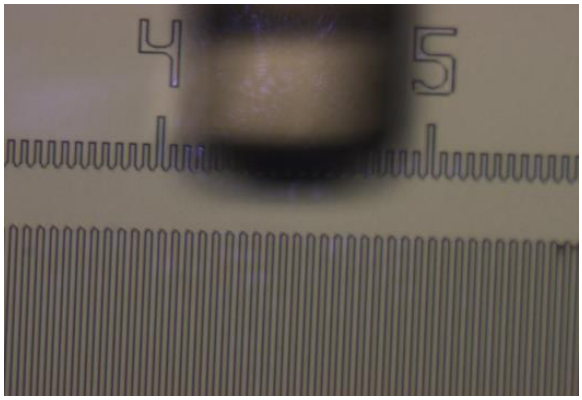

Figure 5.9 MicroMasch TGF11 appearance.

After this step, in order to find the half-width, W, and the offset, Δ, for the flat and for the sloped surface, it is necessary to plot the graph (Figure 5.10) related with the C-D signal (LFM graph in LabVIEW™ interface – Figure 4.8).

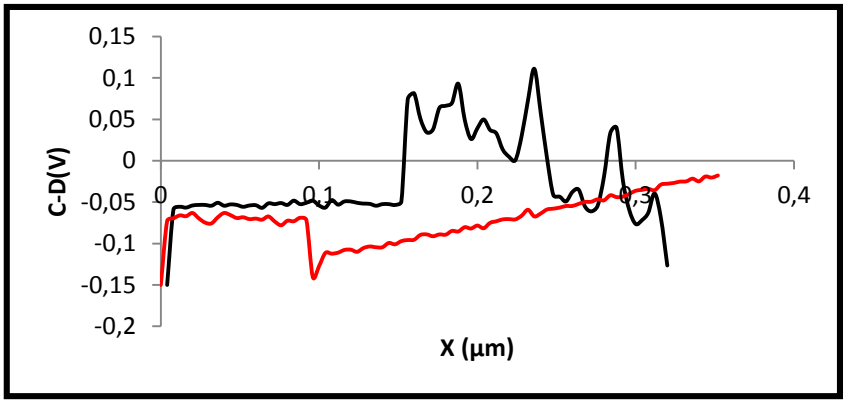

Figure 5.10 C-D signal after scanning the calibration sample.

There are two other graphs that may be interesting to show, which are the ones about the Z-axis displacement and also the C-D signal (they are superposed – Figure 5.11). It shows the profile of the sample (with several bumps, as previously said).

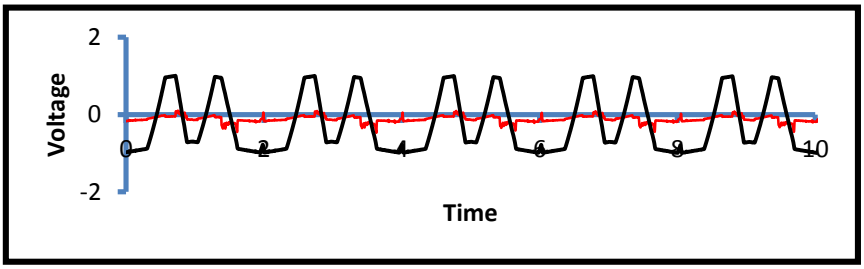

Figure 5.11 C-D and Z displacement signals superposed.

The graph shown in Figure 5.10 is, to some extent, an extract of the graph presented above.

Now that all the information necessary to find the half-width and the offset is available, let's obtain their respective values, from Figure 5.10 (these values were directly calculated and then extracted with Excel, instead of finding M_s, m_s, M_f and m_f (average of the voltage in all situations)):

- W_{slope}: 0.004646
- W_{flat}: -0.07643
- Δ_{slope}: -0.0659
- Δ_{flat}: -0.0528

There is another parameter that also needs to be known, and it is given by XEI, which is the adhesion force, A. This factor is obtained when the user performs a nano-indentation. In this case, it is equal to 2.09 μN

Then, these values are replaced on equation (4.8):

$$sin\theta(Lcos\theta + A)\mu_w^2 - \frac{\Delta_{slope} - \Delta_{flat}}{W_{slope}}(Lcos\theta + A)\mu_w + Lcos\theta\ sin\theta = 0$$

and the value for the friction coefficient, μ_w, is attained, which is equal to **0.073 μN** (two positive values were obtained – 0.073 μN and 3.41 μN. The smallest one was considered, because it was the most approximate value compared to the one that David Laot obtained when he did the same approach. Furthermore, his setup was not much different from the one followed in the present text.

Finally, our last variable, **α**, is obtained by replacing μ_w on equation (4.9):

$$\alpha W_{slope} = \frac{(Lcos\theta + A)\mu_w}{cos^2\theta - \mu_w^2 sin^2\theta}$$

The computed value for parameter **α** is **75.782 μN**.

In order to be easier to see all the parameters used in the wedge method Table 5-9 gathers all of them:

Table 5-9 Parameters used in the wedge method.

Variable	Value	Units
Set Point - L	1.2	μN
Slope's Angle - θ	54.44	º (degrees)
Adhesion Force - A	2.09	μN
μ_w	0.073	-
α	75.782	μN/V

Hence, now, the voltage can be finally translated into cutting force, since all the parameters were found.

5.4.1.1. Result analysis

In order to make the translation of the voltage data to cutting force two additional grooves were performed. It was not possible to used the other ones already made (in pure forward direction) because, for instance, the A-B signal is influenced by both the normal and tangential force at the same time and thus, it is not possible to make a distinction between them. In that case, the C-D signal does not correspond to a measure of the tangential force because this force does not exert any torsion on the cantilever with a pure forward direction. Therefore, to overcome this, grooves made at an angle other than 0º, compared to the pure forward direction, were made. In this case, the chosen angle was 20º.

Consequently, as mentioned before, two other grooves were machined in the forward direction: one with a load of 10000 nN (groove 4) and another one with a load of 20000 nN (groove 5) with an angle of 20º. The cantilever and the sample used are the same used for the other grooves: DNISP EB2 (for the cantilever) and Single Crystal Copper (for the sample). The setups used to perform the two mentioned grooves can be seen on Table 5-10:

Table 5-10 Groove 4 and 5 setup used.

Groove	Direction	Set Point [nN]	Max Load [nN]	Velocity [μm/sec]	Angle [degrees]
4	Forward	1500	20000	5	20
5	Forward	1500	10000	5	20

Moreover, to obtain the normal and tangential force of the machined grooves, the graphs corresponding to the A-B and C-D signal of these grooves are then shown, as well as the one regarding the displacement of the Z axis, which allowed me to extract the points just respecting the groove and not all the process, from the approach of the cantilever, till its retraction.

- **GROOVE 4:**

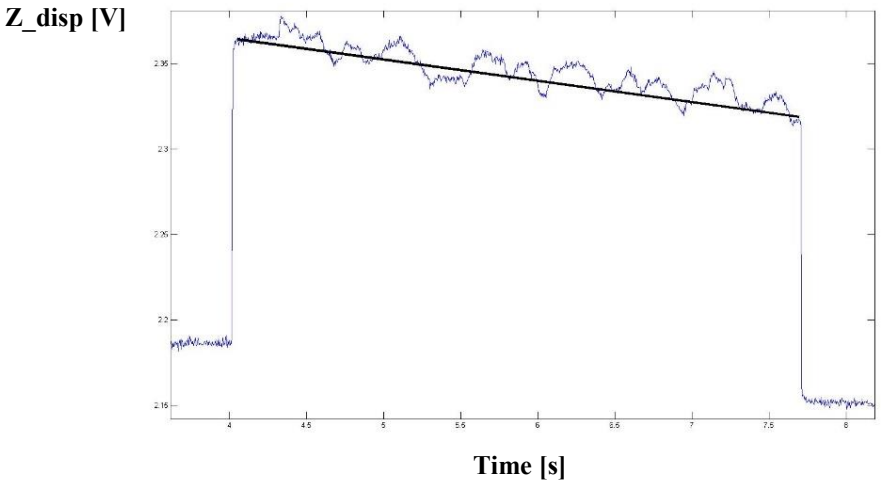

Figure 5.12 Z-axis behaviour.

The graph shown in Figure 5.12 corresponds to the Z-axis displacement during the beginning of the machining process, till its conclusion.

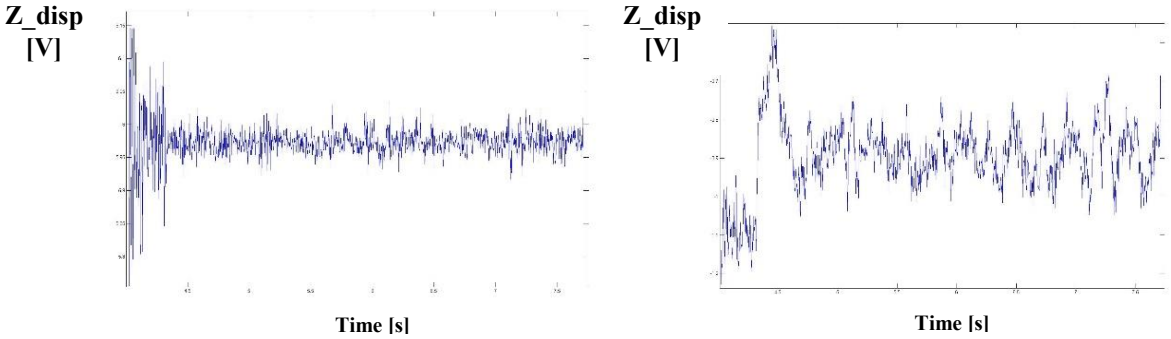

Figure 5.13 A-B (left) and C-D (right) signals for groove 4-

Figure 5.13 shows the signals A-B and C-D just during the scratching process, which correspond to that black line visible on Figure 5.12.

- **GROOVE 5:**

For groove 5 the graphs are the following (Figures 5.14 and 5.15):

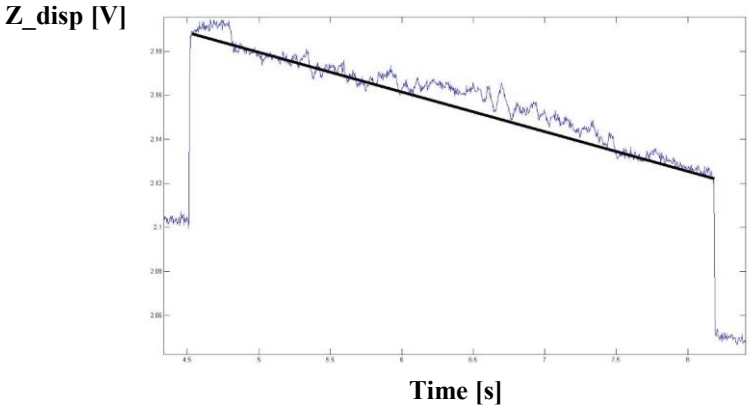

Figure 5.14 Z-axis behaviour-

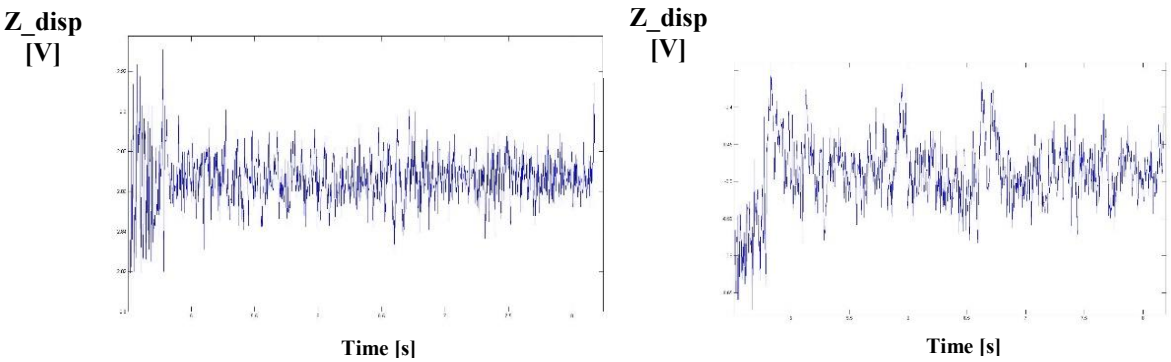

Figure 5.15 A-B (left) and C-D (signals) for groove 5-

Since there are lots of points to consider, the average of each signal (Z_det; A-B; C-D), during the scratching process was computed, as well as the standard deviation. Then, in order to assess whether the attained average can be a trustful parameter, or not, the coefficient of variation (CV) was computed and its result is shown in percentage. The values are shown on Table 5-11.

Table 5-11 Groove 4 and 5 average values, as well as their SD and CV.

Groove	Z_det		A-B		C-D	
	Avg.	**Std. Dev.**	**Avg.**	**Std. Dev.**	**Avg.**	**Std. Dev.**
4	2.345863	0.013909	5.973209	0.030392	0.896032	0.096538
	Coef. Variation (%)					
	0.59%		0.51%		10.77%	
	Z_det		**A-B**		**C-D**	
5	2.159004	0.018793	2.86622	0.013524	0.489369	0.046433
	Coef. Variation (%)					
	0.87%		0.47%		9.47%	

As it is visible, the highest values for the CV are related to the C-D signal and they are equal to 10.77% and 9.47% for groove 4 and 5, respectively. However, since these values are not so low the values of the average can be considered as trustful. Therefore, the values obtained are used to calculate the normal and tangential forces.

Now that all the calibration coefficients were found, they need to be multiplied them by the A-B and C-D data values, considering equations (4.1) and (4.3):

$$F_n = ß \cdot V_{A-B} \text{ and } F_t = \alpha \cdot V_{C-D}$$

Thus, the normal and tangential forces are presented on Table 5-12:

Table 5-12 Normal and Tangential Forces values.

Cutting Force		F_n [µN]	F_t [µN]
Groove	4 (FW 20000, 20º) nN)	22.26	67.9
	5 (FW 10000, 20º) nN)	10.66	37.09

5.4.1.2. **Conclusion**

After applying all the methods thoroughly described in the sections before, it is possible to conclude that, in fact, it is possible to measure the cutting force by monitoring the voltage data. Then the results obtained allow us to confirm the validity of the methods applied. As it can be seen on Table 6-12, the attained values are very close to the initial load values established (10 µN and 20 µN). Therefore, according to the cantilever's deflection (in the case of the Normal Force – A-B signal) and torsion (in the case of Tangential Force – C-D signal) it is possible to translate the voltage data into cutting force. Moreover, the very small difference that it may be observed between the values established in the machining software and the values obtained after computing the cutting force can be related to the errors that the cutting force can exert (i.e. if a high lateral torsion is present, probably higher errors will appear).

6. CONCLUSIONS

This project carried out the studies of using LabVIEW™ for CAD/CAM approaches was carried out. Especially, it was possible to overcome the serious drawbacks that using convention CAD/CAM software suffers, in terms of portability, freedom of motion and flexibility. Two different voltages were sent at the same time, which proves the feasibility of performing much more complex trajectories.

Moreover, the programs made under LabVIEW™ are considered to be the most adequate to test simple and complex trajectories with the possibility of overcoming the physical constraints related to the speed control. Therefore, the mechanism of controlling the time duration, t_f, is considered to be of great relevance to obtain smooth trajectories. In this aspect the application of several mathematical approaches was of great importance to improve the mathematical equations used.

However, it is important to note that this project is not a CAD/CAM project, since its main aim is not the development of a software, but to obtain an efficient machining at nano-scale by a freely range of motion and with a high level of automation using National Instruments LabVIEW™ software. Therefore, this project establishes a first step towards achieving a fully automated CAD/CAM process.

Even the constraints faced during this project allowed to research further. The problems related to the lack of power between the device that would translate the numeric signal into analog signal (DAQ Module 9269) and the Signal Access Module of the AFM, allowed to research further into an area that has a really strong connection with the process of machining as is the case of the evaluation of the quality of the height and width profiles. The pile-ups creation and development, in relation to the application of a low or high load, or even more important, the machining directions were also important properties that were analyzed.

In order to be possible to send the data from LabVIEW™ towards the AFM stage, some solutions were found (see Figure 6.1). Either an Operational Amplifier to increase the power that the cDAQ Module 9174 can supply to the SAM is used, or the PXIe 1071 chassis with the card PXI 6229, which has a higher impedance and can also convert the numeric signal into analog signal, can also be used.

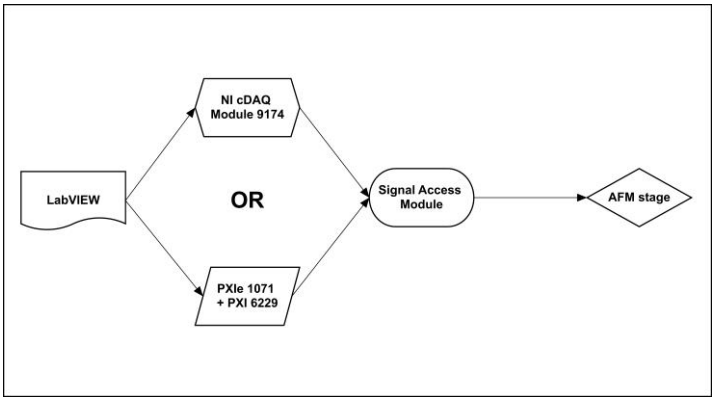

Figure 6.1 Two possibilities for driving the AFM stage.

Another important accomplishment that it was possible to achieve was the validation of the method that allows any user to monitor the voltage data and then translate it into cutting force. This is a really relevant aspect in order to understand the source of errors, which may be caused by the reactions on the cantilever (bending or torsion) in relation to the loads applied.

There are some outlooks that are here suggested as a further development to this project.

In order to validate what has been done in this project concerning the displacement of the nanometric table, it is suggested that further research try to connect all the devices shown in Figure 6.2. With the nanometric table in Lille, using a PXI, which might be a better solution, instead of using the Operational Amplifier. Moreover, further research may be able to both acquire and generate a voltage signal with the programs already available.

In Cardiff, it will be possible, so it is hoped, to connect the devices used in Lille to the AFM stage, that is to say: LabVIEW™ – PXIe 1071 + PXI 6229 – SAM – AFM stage. This should enable the researcher to displace the table and, at the same time acquire and generate a signal, while it is constantly being monitored (see Figure 6.2).

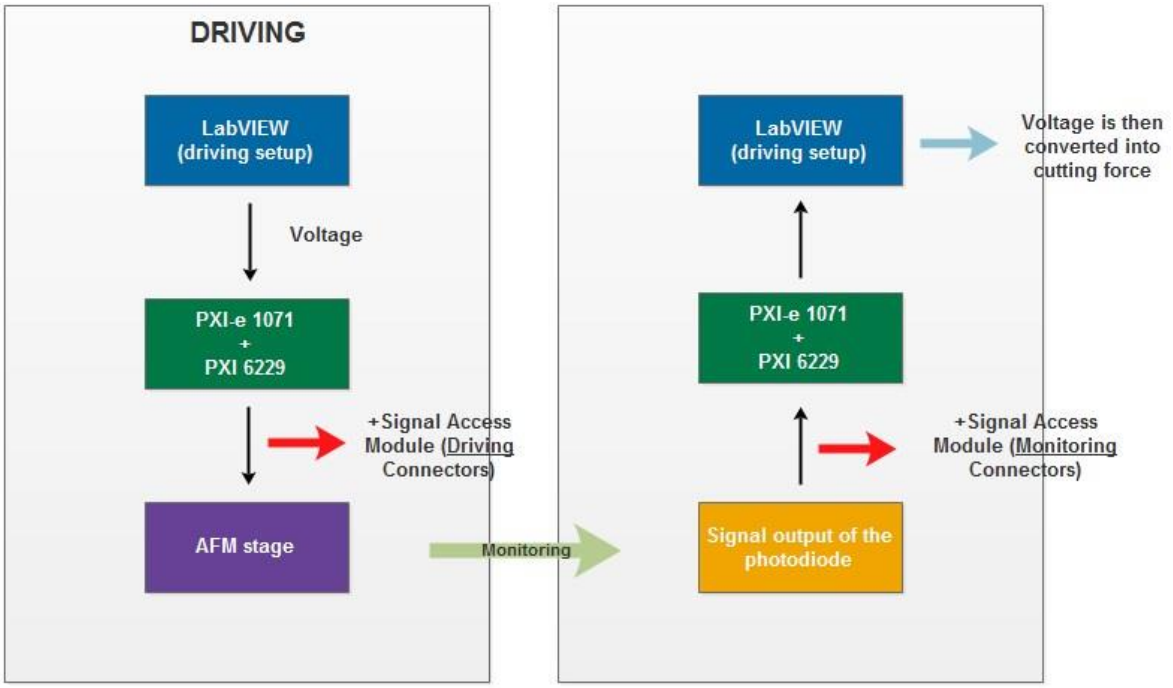

Figure 6.2 Scheme of a suggested interface for driving the AFM and then monitor the signal generated on it

In what regards the evaluation of the grooves machined it is suggested the experiment of machining in the four possible directions: forward/backward and upward/downward with different loads. This will influence the pile-ups formation as well as their width and height profiles. Varying the cantilever's angle in relation to the sample, as well as, the angle of the trajectory may also affect the expected results.

As a final suggestion is the translation of the voltage data obtained with the photodiode, after the machining process.

Moreover, in a long term, all that has been described before should be put into practice and, after achieving a fully automated CAD/CAM process, the source of errors should be very well understood, in order to allow the user to take into consideration this errors in the initial setup and, thus, correct them by anticipation. This will allow the user to obtain the best possible profile.

7. BIBLIOGRAPHY

Binnig, G., & Quate, C. F. (March, 3rd 1986). Atomic Force Microscope. *Physical Review Letters, 56*(9), 930-934.

Brousseau, E. B., Arnal, B., Thiery, S., Nyiri, E., Gibaru, O., & Mayor, J. R. (2013). Towards CNC Automation in AFM Probe-Based Nano Machining. *ICOMM, 95*, 499-506.

Brousseau, E. B., Krohs, F., Caillaud, E., Dimov, S., Gibaru, O., & Fatikow, O. (June, 2010). Microscopy Scratching for Small and Medium Series Production of Polymer Nanostructured Components . *Journal of Manufacturing Science and Engineering, 132*, 030901-8.

Brousseau, E. B., Krohs, F., Caillaud, E., Dimov, S., Gibaru, O., & Fatikow, S. (June, 2010). Development of a Novel Process Chain Based on Atomic Force Microscopy Scratching for Small and Medium Series Production of Polymer Nanostructured Components. *Journal of Manufacturing Science and Engineering, 132*(3), 030901-1;030901-8.

Cannara, J. R., Eglin, M., & Carpick, R. W. (May, 2006). Lateral force calibration in atomic force microscopy: A new lateral force calibration method and general guidelines for optimization. *Review of Scientific Instruments, 77*(5), 1-11.

Corporation, P. S. (2010). Preface. Em P. S. Corporation, *Signal Access Module: Convenient Access to Analog Input and Output Signals of XE Plus Electronic* (Vol. 1.1.0). Suwon, Korea.

Cruchon-Dupeyrat, S., Porthun, S., & Liu, G.-Y. (2001). Nanofabrication using computer-assisted design and automated vector-scanning probe lithography . *Applied Surface Science, 175-176*, 636-642.

Eigler, D. M., & Schweizer, E. K. (April, 1990). Positioning single atoms with a scanning tunneling microscope . *Letters to Nature , 344*, 524-526.

Horcas, I., Fernández, R., Gómez-Rodríguez, J. M., Colchero, J., Gómez-Herrero, J., & Baro, A. M. (2007). WSXM: A software for scanning probe microscopy and a tool for nanotechnology. *Review of Scientific Instruments, 78*(1), 1-8.

Johannes, M. S., Cole, D. G., & Clark, R. L. (2007). Three-dimensional design and replication of silicon oxide nanostructures using an atomic force microscope . *Nanotechnology, 18*, 1-7.

Johannes, M. S., Kuniholm, J. F., Cole, D. G., & Clark, R. L. (July, 2006). Automated CAD/CAM-Based Nanolithography Using a Custom Atomic Force Microscope. *IEEE Transactions on Automation Science and Engineering, 3*(3), 236-239.

Johannes, M. S., Kuniholm, J. F., Cole, D. G., & Clark, R. L. (July, 2006). Automated CAD/CAM-Based Nanolithography Using a Custom Atomic Force Microscope. *IEEE Transactions on Automation Science and Engineering, 3*(3), 236-239.

Jung, T. A., Moser, A., Hug, H. J., Brodbeck, D., Hofer, R., Hidber, H. R., & Schwarz, U. D. (1992). The atomic force microscope used as a powerful tool for machining surfaces . *Ultramicroscopy, 42-44*, 1446-1451.

Kim, Y. S., Na, K. H., Choi, S. O., & Yang, S. H. (2004). Atomic force microscopy-based nano-lithography for nano-patterning: a molecular dynamic study. *Journal of Materials Processing Technology*(155-156), 1847-1854.

Ko, S., & Kim, S.-J. (January, 2009). Transistor characteristics of a parallel-channel and a serial-channel superconducting flux flow transistor fabricated by the AFM anodization process. *Current Applied Physics , 9*(1), S35-S37.

Laot, D. (2013). *Measurement and understanding of path error in nano machining by AFM.* MSc Thesis, Arts et Métiers ParisTech and Cardiff School of Engineering, Lille and Cardiff.

Malekian, M., Park, S. S., Strathearn, D., Mostofa, G. M., & Jun, M. B. (2010). Atomic force microscope probe-based nanometric scribing. *Journal of Micromechanics and Microengineering*, 1-11.

Michaut, P., & Rozier, M. (2014/2015). *Controlle/commande d'une table nanometrique pour l'usinage par AFM.* Arts et Métiers ParisTech Lille, Lille.

Notargiacomo, A., Foglietti, V., Cianci, E., Capellini, G., Adami, M., Faraci , P., . . . Nicolini, C. (1999). Atomic force microscopy lithography as a nanodevice development technique. *Nanotechnology, 10*, 458-463.

Ogletree, D. F., Carpick, R. W., & Salmeron, R. (September, 1996). Calibration of frictional forces in atomic force microscopy . *Rev. Sci. Instrum. , 67*, 3298-3306.

Simões, F. (2011/2012). Tecnologia Mecânica Lessons. Portugal.

Varenberg, M., Etsion, I., & Helpering, G. (July, 2003). An improved wedge calibration method for lateral force in atomic force microscopy. *Review of Scientific Instruments, 74*(7), 3362-3367.

Xie, X. N., Chung, H. J., Sow, C. H., & Wee, A. T. (2006). Nanoscale materials patterning and engineering by atomic force microscopy nanolithography. *Materials Science and Engineering, R*(54), 1-48.

Yan, Y., Sun, T., Liang, Y., & Dong, S. (2007). Investigation on AFM-based micro/nano-CNC machining system. *International Journal of Machine Tools & Manufacture, 47*(11), 1651–1659.